mRNA delivery of mosaic-8 pan-sarbecovirus RBD vaccines elicits distinct antibody epitope signatures

Alexander A. Cohen[1], Jennifer R. Keeffe[1], Lusineh Manasyan[1], Indeever Madireddy[1], Ange-Célia I. Priso Fils[1], Kim-Marie A. Dam[2], Haley E. Stober[2], Rory A. Hills[3,4,7], Woohyun J. Moon[5], Paulo J.C. Lin[5], Mark R. Howarth[3], Magnus A.G. Hoffmann[2,6,8*], Pamela J. Bjorkman[1,8*]

Affiliations

[1]Division of Biology and Biological Engineering, California Institute of Technology, Pasadena, CA 91125, USA

[2]Gladstone Institutes, San Francisco, CA 94158, USA

[3]Department of Pharmacology, University of Cambridge, Tennis Court Road, Cambridge, CB2 1PD, UK

[4]Department of Biochemistry, University of Oxford, Oxford, OX1 3QU, UK

[5]Acuitas Therapeutics, Vancouver, BC, V6T 1Z3, Canada

[6]Department of Medicine, University of California, San Francisco, CA 94143, USA

[7]Present address: Department of Pathology, Stanford University, School of Medicine, Palo Alto, CA 94305, USA

[8]Lead contact

[*]Correspondence: magnus.hoffmann@gladstone.ucsf.edu, bjorkman@caltech.edu

Keywords

epitope mapping; mRNA and protein nanoparticle vaccines; pandemic preparedness; pan-sarbecovirus vaccine; systems serology; SySPEM (systems serology-polyclonal epitope mapping)

Abstract

Effective pan-sarbecovirus vaccines could prevent future zoonotic spillovers of SARS-like betacoronaviruses. We previously developed protein-based mosaic-8 nanoparticles displaying eight diverse sarbecovirus RBDs, either individually (mosaic-8 RBD-NPs) or as two "quartets" of four tandemly-arranged RBDs (dual-quartet RBD-NPs), which elicited broadly cross-reactive antibodies but require multi-component manufacturing. Here, we address scalability challenges by extending the mosaic-8 concept to mRNA by encoding membrane-bound RBD quartets as dual-quartet RBD-mRNA and dual-quartet RBD-EABR-mRNA, the latter leveraging ESCRT- and ALIX-binding region (EABR) technology for immunogen display on cell surfaces and secreted virus-like particles. Compared with protein-based mosaic-8 immunogens, mRNA-encoded mosaic-8 vaccines induced equivalent or enhanced antibody breadth, neutralization potencies, T-cell responses, and targeting of conserved RBD epitopes. In addition, mRNA-encoded mosaic-8 vaccines elicited more balanced IgG subclass profiles and increased Fcγ receptor–binding IgGs, consistent with potentially superior Fc effector functions. These findings demonstrate successful translation of mosaic-8 RBD-NPs into mRNA/EABR-mRNA vaccines, enabling scalable manufacturing and improving protection against future sarbecovirus outbreaks. Finally, our newly developed technique, Systems Serology–Polyclonal Epitope Mapping (SySPEM), revealed distinct IgG-subclass-specific epitope signatures across mRNA, EABR-mRNA, and protein vaccines, demonstrating that the mode of antigen display can shape epitope recognition.

Summary

We translated a pan-sarbecovirus RBD vaccine from protein nanoparticles to scalable mRNA and EABR-mRNA platforms encoding RBD quartets. Compared with protein-based immunogens, mRNA-based vaccines matched or improved antibody breadth, T-cell responses, Fc functionality, and conserved epitope targeting. A newly-developed Systems Serology–Polyclonal Epitope Mapping (SySPEM) technique revealed that antigen presentation modality shapes IgG subclass–specific epitope recognition.

Introduction

Three coronaviruses spilled over from animal hosts to cause human epidemics or pandemics in the past 25 years: SARS-CoV (hereafter SARS-1), MERS-CoV, and SARS-CoV-2 (hereafter SARS-2) (Andersen et al., 2020). Two of these, SARS-1 and SARS-2, are members of the SARS-like betacoronavirus (sarbecovirus) subgenus. SARS-2 continues to infect humans, driving emergence of new variants that necessitate regular updates of current COVID-19 vaccines (Roederer et al., 2024). Since we cannot predict how SARS-2 will continue to mutate or which zoonotic sarbecovirus will next infect humans, we need a pan-sarbecovirus vaccine that does not require updating to provide broad protection against new SARS-2 variants and future sarbecovirus spillovers (Whittaker et al., 2025).

Spike trimers of coronaviruses function in host cell entry after one or more receptor-binding domains (RBDs) adopt an "up" position to permit interactions with a host receptor (Hills et al., 2025). RBD targeting has been suggested for COVID-19 vaccine development as RBDs are the main target of neutralizing antibodies (Abs) (Kleanthous et al., 2021). We previously described a vaccine approach that elicits broad Ab responses to diverse sarbecoviruses involving RBDs from multiple sarbecoviruses that are covalently linked using the SpyCatcher-SpyTag system (Bruun et al., 2018) to a SpyCatcher-mi3 protein nanoparticle (NP) (Cohen et al., 2021a; Cohen et al., 2024; Cohen et al., 2022; Wang et al., 2025). In this approach, mosaic-8 RBD-NPs displayed eight different sarbecovirus spike RBDs attached randomly to the 60 positions of the mi3 NP (Fig. 1, A and B). We hypothesized that B cells bearing cross-reactive receptors (B cell receptors; BCRs) recognizing features in common between adjacent non-identical RBDs are preferentially activated compared to B cells with BCRs recognizing immunodominant strain-specific epitopes (Cohen et al., 2022) (Fig. 1 A). To investigate this, we used deep mutational scanning (DMS) (Starr et al., 2020) to map RBD epitopes recognized by Abs from animals immunized with mosaic-8 RBD-NPs or homotypic RBD-NPs (only presenting SARS-2 RBD), revealing targeting of more conserved RBD regions by mosaic-8 RBD-NP–elicited Abs compared with targeting of more variable RBD regions by homotypic RBD-NP–elicited Abs (Cohen et al., 2025; Cohen et al., 2024; Cohen et al., 2022; Hills et al., 2024; Wang et al., 2025). This finding rationalized results from challenge experiments in which mosaic-8 RBD-NPs protected from both a matched viral challenge (from a virus represented by an RBD on the NP) and a mismatched challenge (from a virus not represented by an RBD on the NP), whereas homotypic RBD-NPs protected only from a matched challenge (Cohen et al., 2022). We also found broader Ab responses elicited by mosaic-8 RBD-NPs in animals that were pre-vaccinated with COVID-19 vaccines (Cohen et al., 2024). These results suggest that a mosaic-8 RBD-based vaccine given as a COVID-19 booster could provide increased protection from SARS-2 variants and prevent future sarbecovirus spillover(s) from causing an epidemic or pandemic.

Manufacturing a mosaic-8 RBD-NP vaccine would require producing nine proteins: eight RBDs and a NP to which the RBDs are coupled. Making an mRNA-based version of a mosaic-8 vaccine would also pose challenges due to the requirement of synthesizing eight individual modified mRNAs. The RBD-encoding mRNAs could either be packaged into individual lipid nanoparticles (LNPs) or co-formulated into a single LNP. In the first case, some cells would not take up all eight mRNA LNPs, therefore presenting fewer instances of different adjacent RBDs, potentially reducing avidity effects to activate B cells with maximally cross-reactive BCRs (Fig. 1 A). In the second case, co-formulation of eight mRNAs into a single LNP would present technical and regulatory challenges. A potential solution relevant to converting a mosaic-8 vaccine into an mRNA format involves making mi3 NPs presenting two RBD "quartets" (each containing four RBDs arranged in tandem), which elicit equally broad and potent Abs as the original mosaic-8

RBD-NP presenting monomeric RBDs (Hills et al., 2024) (Fig. 1 C; dual quartet RBD-NP). Dual quartet RBD-NPs require manufacture of only three components (two quartets and a NP), and by synthesizing mRNAs encoding membrane-bound RBD quartets, could be more easily converted to an mRNA-LNP format than mosaic-8 RBD-NPs. In addition to simpler manufacturing, mRNA-LNP vaccines offer advantages over protein-based vaccines in that viral antigens undergo translation in the cytoplasm, thereby providing a source of viral peptides for presentation by MHC class I molecules to activate CD8+ cytotoxic T cells (Gote et al., 2023).

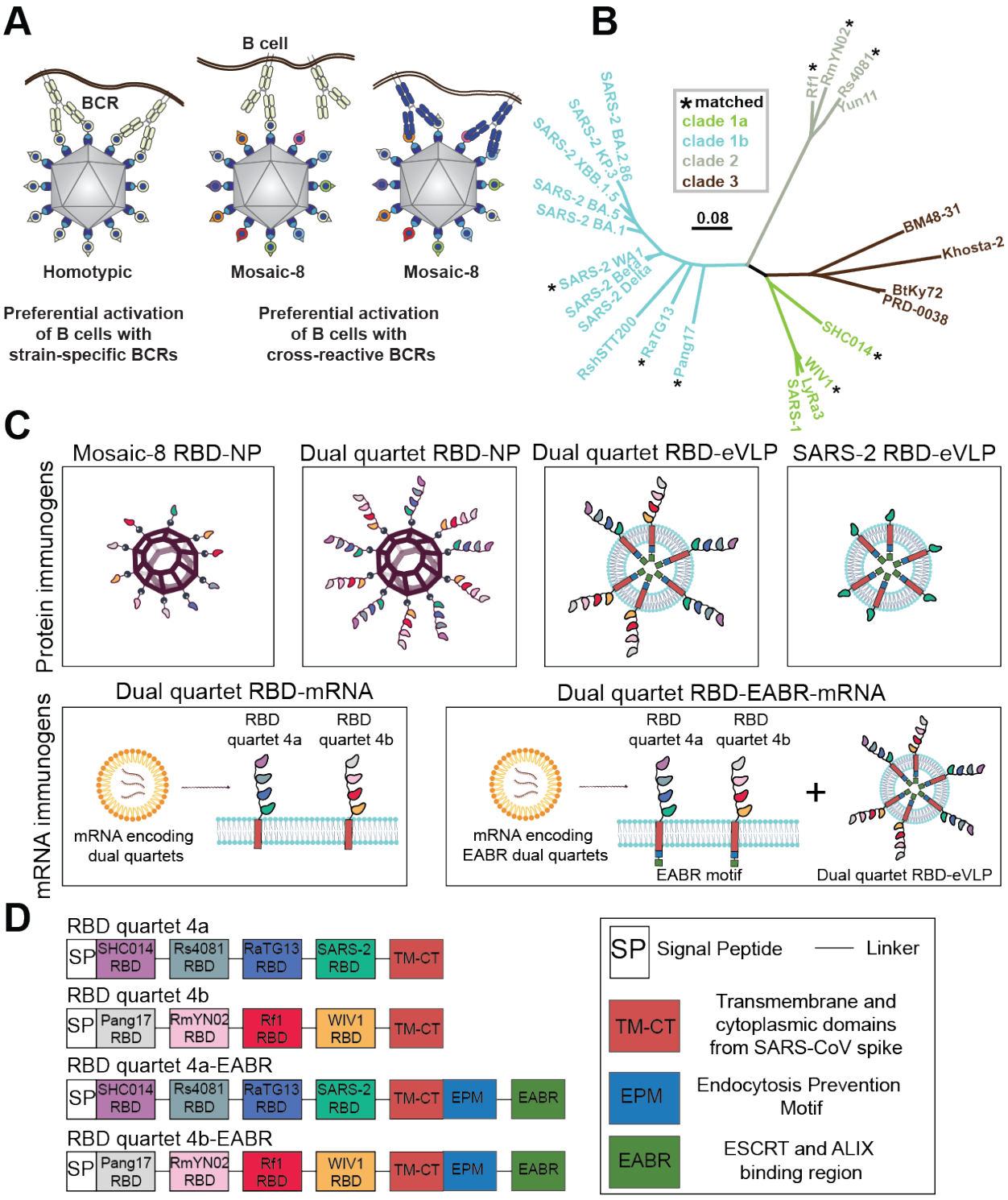

Figure 1. Protein- and mRNA-based pan-sarbecovirus immunogens.
(A) Avidity hypothesis. Left: Membrane-bound strain-specific BCRs (pale yellow) using avidity to recognize a strain-specific epitope (pale yellow triangle) on antigens attached to a homotypic NP. Middle: Strain-specific BCRs binding with only a single Fab (i.e., not using avidity) to a strain-specific epitope (triangle) on an antigen attached to a mosaic NP. Right: Cross-reactive BCRs using avidity to recognize a common epitope (blue circle) presented on different antigens attached to a mosaic NP, but not to strain-specific epitopes (triangles). Only a fraction of the 60 attached RBDs are shown for clarity. (B) Sarbecovirus phylogenetic tree (made using a Jukes-Cantor generic distance model with Geneious Prime® 2023.1.2) calculated from amino acid sequences of RBDs aligned using Clustal Omega (Sievers et al., 2011). Viruses with RBDs included in RBD quartets and mosaic-8 RBD-NPs are indicated with an asterisk. Scale bar = phylogenetic distance of 0.08 nucleotide substitutions per site. (C) Schematics of protein-based and mRNA-based pan-sarbecovirus immunogens (not to scale; showing only a fraction of antigens for clarity). (D) Schematics of mRNA constructs encoding RBD dual quartet immunogens used in this study.

Conversion of dual RBD quartet immunogens to an mRNA format (Fig. 1 C; dual quartet RBD-mRNA) is also compatible with using the ESCRT- and ALIX-binding region (EABR) mRNA vaccine platform, which presents immunogens on cell surfaces and on circulating enveloped virus-like particles (eVLPs), thereby combining attributes of both mRNA and protein-NP vaccines (Hoffmann et al., 2023) (Fig. 1 C; dual quartet RBD-EABR-mRNA). eVLP formation is achieved by appending an EABR sequence to the cytoplasmic domain of the mRNA-encoded immunogen, which recruits cellular ESCRT proteins to induce eVLP budding from the plasma membrane. We previously showed that two immunizations with mRNA-LNPs encoding spike-EABR elicited potent CD8+ T-cell responses and superior neutralizing Ab responses against original and variant SARS-2 compared to conventional spike-encoding mRNA-LNPs, improving neutralizing titers >10-fold against Omicron-based variants (Hoffmann et al., 2023).

Until this study, it was not known whether presentation of membrane-bound RBD quartets on eVLPs and/or the surfaces of cells would elicit cross-reactive Abs to the extent we observed using RBD quartets or single RBDs covalently linked to rigid protein NPs. Here, we show that the advantages of protein-based mosaic-8 RBD-NPs can be transferred to an mRNA-LNP format. We compared immune responses in mice immunized with dual quartet RBD-mRNA versions of mosaic-8 immunogens (dual quartet RBD-mRNA and dual quartet RBD-EABR-mRNA) with responses to two protein-based mosaic-8 NPs (dual quartet RBD-NPs (Hills et al., 2024) and EABR-based dual quartet RBD-eVLPs) or to homotypic SARS-2 RBD-eVLPs. Immunization with mRNA immunogens elicited equivalent or improved binding breadths, neutralization potencies, T cell responses, and targeting of conserved RBD epitopes across sarbecoviruses compared to protein-based mosaic-8 immunogens, demonstrating successful conversion of the mosaic-8 RBD vaccine to mRNA formats that enable streamlined, scalable manufacturing of a pan-sarbecovirus vaccine.

Results

mRNA-encoded RBD quartets are presented on cell surfaces and eVLPs

mRNA-LNPs direct cell surface expression of a variety of gene products, including viral antigens (Hou et al., 2021). We investigated whether protein-based soluble dual quartets could be modified

138 to induce cell surface expression by creating constructs that encode an RBD quartet followed by a
139 linker, transmembrane anchoring sequence, and cytoplasmic tail (Fig. 1 D; RBD quartets 4a and
140 4b). The eight RBDs in the 4a and 4b quartet sequences correspond to the RBDs used in previous
141 studies of protein-based dual quartet RBD-NPs (Hills et al., 2024) and to RBDs in a mosaic-8
142 RBD-NP constructed from soluble monomeric RBDs (Cohen et al., 2021a) (Fig. 1 B). We used
143 flow cytometry to verify presentation of membrane-bound RBD quartets on the surface of cells
144 transfected with mRNA encoding RBD quartets 4a or 4b by staining with C118, a human mAb
145 that recognizes a conserved RBD epitope present on all eight RBDs (Jette et al., 2021; Robbiani
146 et al., 2020). Flow cytometry showed high and equivalent levels of RBD quartets 4a and 4b on cell
147 surfaces when expressed separately (Fig. S1 A).
148
149 We next investigated use of EABR technology, which modifies membrane proteins delivered by
150 mRNA-LNPs to induce self-assembly and budding of eVLPs, resulting in immunogen presentation
151 on cell surfaces and circulating eVLPs (Hoffmann et al., 2023), for delivering quartet RBD
152 sequences. eVLPs are induced by appending a short sequence to the cytoplasmic domain of a
153 membrane protein, which recruits proteins from the host ESCRT pathway that drives budding for
154 many enveloped viruses (Votteler and Sundquist, 2013). Addition of an EABR sequence produces
155 eVLPs for a variety of membrane proteins including SARS-2 spike (Hoffmann et al., 2023), HIV-
156 1 Env (Hoffmann et al., 2023), influenza hemagglutinin (Zhang et al., 2025), RSV fusion protein
157 (Chai et al., 2025), Andes virus glycoprotein (Guo et al., 2025), CCR5 (Hoffmann et al., 2023),
158 epidermal growth factor receptor (Gonzalez-Magaldi et al., 2025), and MHC class I proteins
159 (Olson et al., 2025). Compared to non-EABR RBD quartets, cells expressing EABR-modified
160 RBD quartets showed lower cell surface expression (Fig. S1 A), which presumably results from a
161 subset of cell surface proteins being incorporated into released eVLPs.
162
163 To evaluate whether the RBD quartet 4a-EABR and 4b-EABR constructs induced secretion of
164 RBD quartet-displaying eVLPs, we examined eVLPs purified from supernatants of quartet 4a- or
165 4b–transfected cells. ELISAs were consistent with efficient eVLP formation for EABR mRNAs,
166 showing high quartet 4a or 4b protein levels in purified eVLP samples for EABR, but not non-
167 EABR, quartets (Fig. S1 B). We also used Abs specific for quartet 4a (anti-Rs4081 RBD) (Fan et
168 al., 2025b) and 4b (anti-WIV1 RBD) (Fan et al., 2022) to examine co-transfected cells by flow
169 cytometry, demonstrating that RBD quartets 4a and 4b were co-expressed at individual cell
170 surfaces (Fig. S1 C). To confirm that both quartets were incorporated into the same eVLP, we used
171 a sandwich ELISA to probe eVLPs from an RBD quartet 4a-EABR and 4b-EABR co-transfection.
172 eVLPs were purified, captured with anti-WIV1 RBD Ab (quartet 4b), and detected with anti-
173 Rs4081 RBD Ab (quartet 4a), verifying the presence of both quartets on dual quartet eVLPs (Fig.
174 S1 D). No binding was detected for samples prepared in the same way from cells co-transfected
175 with non-EABR versions of the quartets or cells only transfected with a single quartet (Fig. S1 D).
176 These data show that mRNA-encoded RBD quartets are co-expressed on transfected cells and that
177 the two EABR-modified quartets are co-displayed on eVLPs.
178
179 **Dual quartet RBD mRNA immunogens elicit cross-reactive Abs**
180 We next compared Ab responses in mice immunized with mRNA-encoded dual quartets to
181 immunizations with protein-based dual quartet RBD-NPs or with purified dual quartet RBD-
182 eVLPs. mRNAs encoding RBD quartets 4a and 4b were co-formulated into lipid nanoparticles
183 (LNPs) to generate dual quartet immunogens (dual quartet RBD-mRNA and dual quartet RBD-
184 EABR-mRNA), which were each injected intramuscularly at RNA doses of 1.5 µg or 0.5 µg (Fig.
185 2 A, Fig. S2 A). We also included cohorts of mice that were immunized with 5 µg of dual quartet
186 RBD-NPs (calculated based on RBD content) in the presence of adjuvant (Fig. 2 A) and cohorts

immunized with adjuvanted purified RBD-eVLPs (dual quartet RBD-eVLP or SARS-2 RBD-eVLP; 5 µg RBD content per dose), the latter representing a homotypic immunogen control presenting only one type of RBD (Fig. 1 C).

Since binding and neutralizing Ab responses correlate with protection in humans and animals vaccinated with COVID-19 mRNA vaccines (Corbett et al., 2021; Gilbert et al., 2022; Goldblatt et al., 2022), we analyzed immunized mouse sera by ELISA and pseudovirus assays (Schmidt et al., 2020) to evaluate Ab binding responses and neutralization, respectively (Fig. 2, B and C; Fig. S2 B). When comparing mRNA-based to protein-based immunogens, we used a 1.5 µg mRNA dose and a 5 µg (RBD content) dose for the protein-based immunogens (Fig. 2, B and C), representing standard doses in mice (Cohen et al., 2021a; Corbett et al., 2020; Hoffmann et al., 2023). We also compared the mRNA and mRNA-EABR immunogens using a 0.5 µg mRNA dose to investigate potential dose-sparing effects (Fig. S2 B). To evaluate sarbecovirus strain-specific differences in Ab binding and neutralization properties, we displayed data to show responses to individual sarbecovirus antigens (Fig. 2, B and C; left panels) and as overall geometric mean (geomean) responses elicited by different cohorts across evaluated antigens (Fig. 2, B and C; right panels).

Highest mean binding titers for sera across a panel of matched and mismatched sarbecovirus RBDs were found for dual quartet RBD-mRNA and dual quartet RBD-EABR-mRNA cohorts (Fig. 2 B, left). Thus, genetically-encoded RBD quartets delivered by a 1.5 µg dose of mRNA-LNPs were significantly more effective at eliciting cross-reactive RBD-binding Abs across a panel of sarbecovirus RBDs than 5 µg of the dual quartet RBD-NP protein-based immunogen (Fig. 2 B, right; $p<0.0001$ for comparisons of dual quartet RBD-mRNA and dual quartet RBD-EABR-mRNA). In addition, both dual quartet RBD-mRNA and dual quartet RBD-EABR-mRNA exhibited significantly higher geomean binding titers than the protein-based dual quartet RBD-eVLPs and homotypic SARS-2 RBD-eVLPs (Fig. 2 B, right; $p<0.0001$ for all comparisons of mRNA-LNP and protein-based immunogens). SARS-2 RBD-eVLPs exhibited significantly lower binding titers across the RBD panel than the dual quartet RBD-NPs and purified dual quartet RBD-eVLPs (Fig. 2 B, right; $p<0.0001$ for all comparisons except $p=0.0057$ for dual quartet RBD-eVLP), as expected based on results for homotypic RBD-NPs (Cohen et al., 2021a; Cohen et al., 2022).

We next compared neutralizing titers across a panel of matched and mismatched sarbecovirus strains (Fig. 2 C, left). When comparing by strain between the five immunization cohorts, dual quartet RBD-mRNA, dual quartet RBD-EABR-mRNA, and dual quartet RBD-NP exhibited the highest titers across the pseudovirus panel except for neutralization of SARS-2 D614G, where homotypic SARS-2 RBD-eVLPs elicited slightly higher titers (Fig. 2 C, left). Geomean neutralization titers for the five cohorts (Fig. 2 C, right) were more similar to each other than the mean binding titers (Fig. 2 B, right) but dual quartet RBD-EABR-mRNA induced significantly higher mean neutralizing titers than dual quartet RBD-NP ($p=0.0152$), dual quartet RBD-eVLP ($p=0.0152$), and SARS-2 RBD-eVLP ($p=0.0470$).

We also measured binding and neutralization titers elicited by 0.5 µg doses of dual quartet RBD-mRNA and dual quartet RBD-EABR-mRNA (Fig. S2, A and B). Binding titers against the RBDs tested were not statistically different for the two mRNA immunogens, except for binding to the BM48-31 RBD, in which case dual quartet RBD-EABR-mRNA induced significantly higher binding than dual quartet RBD-mRNA (Fig. S2 B, left; $p=0.0089$). Neutralization titers were significantly different for three viruses: SARS-2 D614G (titers higher for dual quartet RBD-

mRNA; p=0.00013) and for SARS-1 and WIV1 (higher for dual quartet RBD-EABR-mRNA; p=0.00024 and p<0.0001, respectively) (Fig. S2 B, right panel). These results are consistent with more potent neutralization of non-SARS-2 viruses induced by dual quartet RBD-EABR-mRNA compared with dual quartet RBD-mRNA at the 1.5 µg dose (Fig. 2 C).

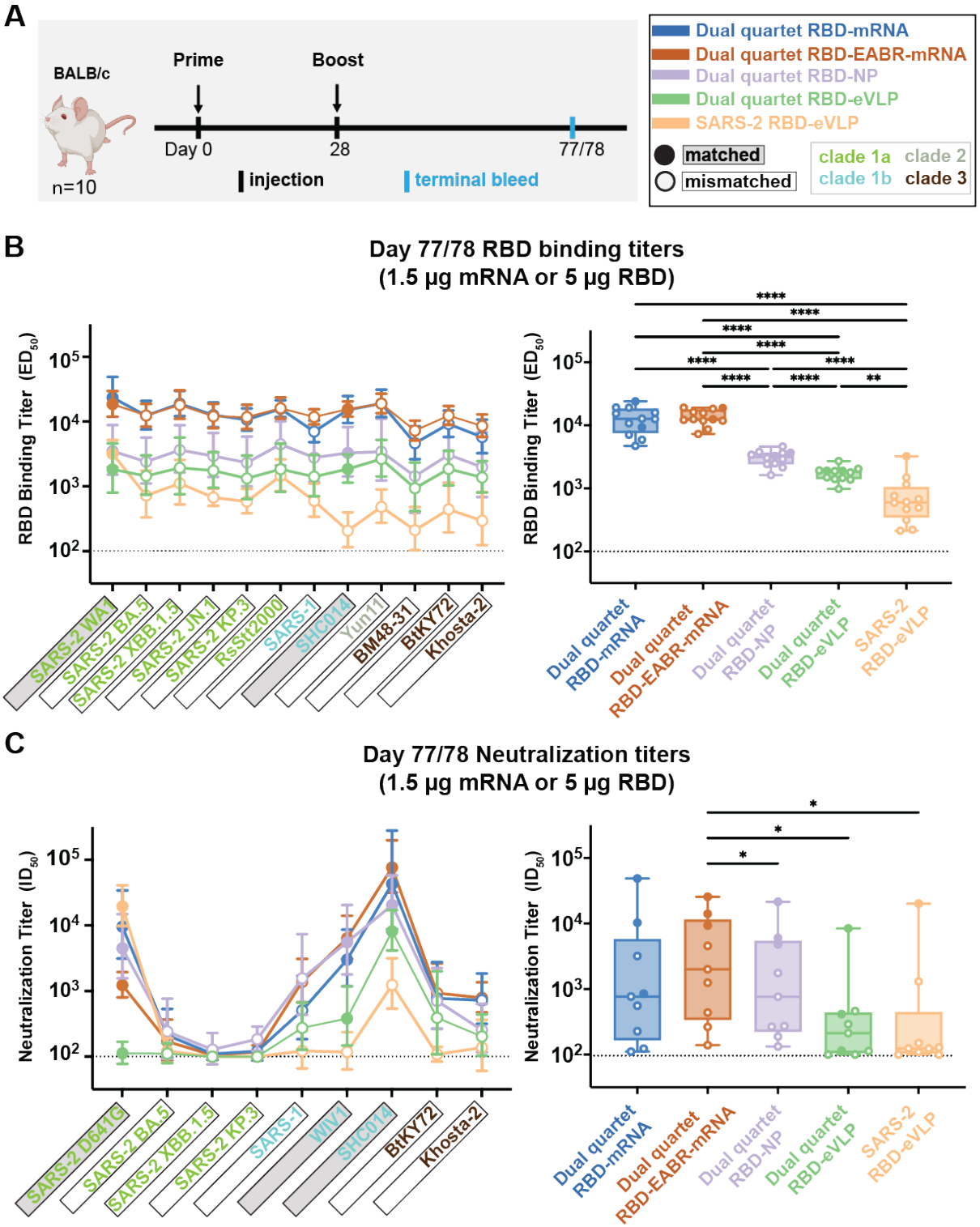

Figure 2. Dual quartet RBD mRNA immunogens elicit cross-reactive Abs.

ELISA and neutralization results for terminal bleed serum samples (see also Fig. S2). (A) Immunization regimen. Left: Mice were primed at day 0, boosted at day 28, and samples were collected from a terminal bleed at day 77 or 78. Right: Colors used to identify immunization cohorts and symbols indicating a sarbecovirus antigen or pseudovirus that is matched (filled in data points; gray shading around name) or mismatched (unfilled data points; black outline around name). Sarbecovirus strain names are colored in panels B and C according to clade. (B,C) Results for RBD-binding ELISAs (panel B) and pseudovirus neutralization assays (panel C) for serum samples from day 77 or 78. Dashed horizontal lines indicate detection limits for assays. Left: Geomeans of RBD-binding ELISA half-maximal effective dilution (ED_{50}) values (panel B) or neutralization half-maximal inhibitory dilution (ID_{50}) values (panel C) across a panel of viral antigens or pseudoviruses for sera from animals in each cohort (geomeans are plotted as symbols with geometric standard deviations indicated by error bars). Mean ED_{50} or ID_{50} values across antigens are connected by colored lines corresponding to the immunization cohort. Right: Box and whisker plots of geomean responses (ELISA ED_{50}s in panel B; neutralization ID_{50}s in panel C) with individual data points representing geomean responses across n=10 sera to a single antigen or pseudovirus. Geomean titers were compared pairwise between immunization cohorts by Tukey's multiple comparison test with the Geisser-Greenhouse correction (as calculated by GraphPad Prism). Significant differences between cohorts are indicated by asterisks: $p<0.05$ = *, $p<0.01$ = **, $p<0.001$ = ***, $p<0.0001$ = ****.

mRNA-encoded dual quartets elicit potent T cell responses

T cell responses to the various immunogens were evaluated on day 77/78 in immunized mouse splenocytes by ELISpot (Ranieri et al., 2014). Cytokines (IFN-γ produced by CD4+ T helper 1 (T_H1) cells and cytotoxic CD8+ T cells; IL-4 produced by CD4+ T helper 2 (T_H2) and T follicular helper cells (Leehan and Koelsch, 2015)) were measured after stimulation with a pool of SARS-2 spike peptides.

Dual quartet RBD-mRNA and dual quartet RBD-EABR-mRNA cohorts exhibited potent IFN-γ responses, consistent with activation of RBD-specific cytotoxic CD8+ T cells, whereas low/undetectable IFN-γ responses were found for the protein-based dual quartet RBD-NP, dual quartet RBD-eVLP, and SARS-2 RBD-eVLP cohort~~s~~, consistent with previous findings for mice immunized with purified spike-EABR eVLPs (Hoffmann et al., 2023) and the fact that mRNA-LNPs, but not protein immunogens, promote intracellular expression of antigens that serve as sources for peptides loaded onto MHC class I proteins (Rock et al., 2016). We found strong IL-4 responses for both the mRNA and protein-based immunogen cohorts (Fig. 3).

Thus, mRNA-based mosaic-8 dual RBD quartet immunizations induce superior (INF-γ) or equivalent (IL-4) release of cytokines compared with protein-based mosaic-8 immunogens.

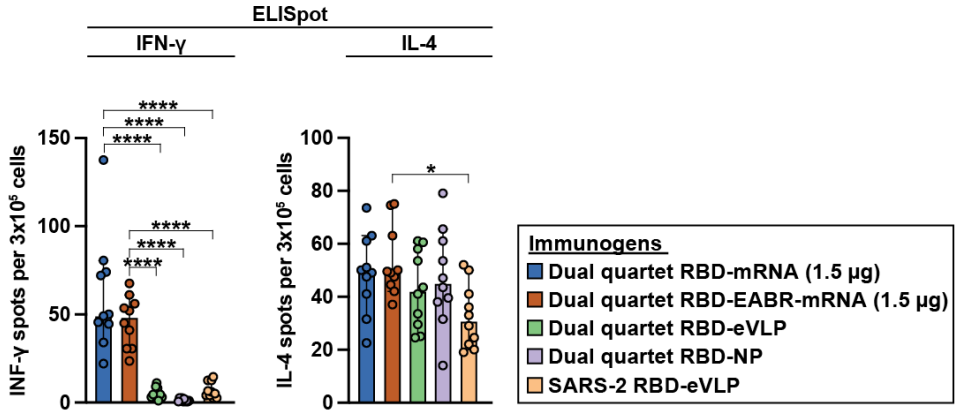

Figure 3. mRNA-encoded dual quartets elicit potent T cell responses. ELISpot assay data for SARS-2 RBD-specific IFN-γ (left) and IL-4 (right) responses of splenocytes from BALB/c mice that were immunized with the indicated immunogens (immunization regimen in Fig. 2 A). Results are shown as spots per $3x10^5$ cells for individual mice (colored circles) presented as the median (bars) and standard deviation (horizontal lines). Cohorts were compared by Tukey's multiple comparison test calculated by GraphPad Prism. Significant differences between cohorts linked by horizontal lines are indicated by asterisks: $p<0.05$ = *, $p<0.0001$ = ****.

mRNA-encoded and protein-based dual quartets elicit Abs targeting similar epitopes

To map RBD epitopes targeted by Abs elicited by different vaccine modalities, we used DMS to evaluate effects of all possible RBD amino acid changes on binding to polyclonal serum Abs (Greaney et al., 2021a; Greaney et al., 2021b; Greaney et al., 2021c; Greaney et al., 2021d; Starr et al., 2021a; Starr et al., 2021b; Starr et al., 2020). We classified RBD residues by epitopes defined by structural properties and conservation/variability across sarbecoviruses: class 1 and class 2 RBD epitopes exhibit more, and class 4, class 1/4, and portions of class 3 and class 5 epitopes exhibit less, sequence variability across sarbecoviruses and SARS-2 variants (Barnes et al., 2020; Cui et al., 2024; Jensen et al., 2023; Jette et al., 2021) (Fig. 4 A). We analyzed serum using yeast display libraries encoding RBDs derived from SARS-2 WA1 (matched) and SARS-1 (mismatched) spikes.

DMS showed that the epitopes targeted in both RBD libraries by the mRNA-encoded dual quartet RBD immunogens were similar overall to each other and to epitopes targeted by the protein-based dual quartet RBD-NP immunogen (Fig. 4, B and C; Table 1; Figs. S3 and S4). The dual quartet immunogens, like mosaic-8 RBD-NPs (Cohen et al., 2024; Cohen et al., 2022), did not primarily elicit Abs against the immunodominant and variable class 1 and class 2 RBD epitopes, as observed for Abs elicited by homotypic SARS-2 RBD NPs (Cohen et al., 2024; Cohen et al., 2022) and spike-based mRNA vaccines (Bangaru et al., 2025). Instead, elicited Abs primarily targeted class 4 and class 5 RBD epitopes, except for the Abs raised by immunization with dual quartet RBD-NPs, where class 5 was the predominant targeted epitope.

Although dual quartet RBD immunizations resulted in a mixed class 4/class 5 RBD response when evaluated against the SARS-2 WA1 and SARS-1 RBD libraries (Fig. 4, B and C; Table 1; Figs. S3 and S4), there were notable differences. For example, both RNA-based immunogens elicited similar class 4 and class 5 RBD responses, but dual quartet RBD-mRNA sera showed more of a class 1/class 2 RBD response than dual quartet RBD-EABR-mRNA sera against the SARS-2 WA1 RBD library (Fig. 4 B and Table 1), perhaps explaining why dual quartet RBD-mRNA elicited higher neutralization titers against the matched SARS-2 D614G pseudovirus (Fig. 2 C and Fig. S2

B). Against the SARS-1 RBD library, each of the dual quartet immunogens induced strong class 4 and class 5 responses. In addition, weak escape by Abs against the variable class 1 and class 2 RBD epitopes was seen for dual quartet RBD-mRNA, dual quartet RBD-EABR-mRNA, and dual quartet RBD-NP (Table 1). Finally, one mouse in the dual quartet RBD-EABR-mRNA group and two in the dual quartet RBD-NP group elicited "polyclass" responses (defined as weak escape profiles that lacked clear features, which we interpret as resulting from sera containing multiple classes of anti-RBD Abs (Cohen et al., 2024), consistent with the ability of these immunogens to induce Abs against multiple RBD epitopes.

We conclude that converting dual quartet RBD immunogens into an mRNA format retains the ability of mosaic-8 vaccines to elicit Abs mainly against more conserved RBD regions, as previously observed in DMS experiments comparing protein NPs presenting dual RBD quartets or eight individual RBDs (Hills et al., 2024).

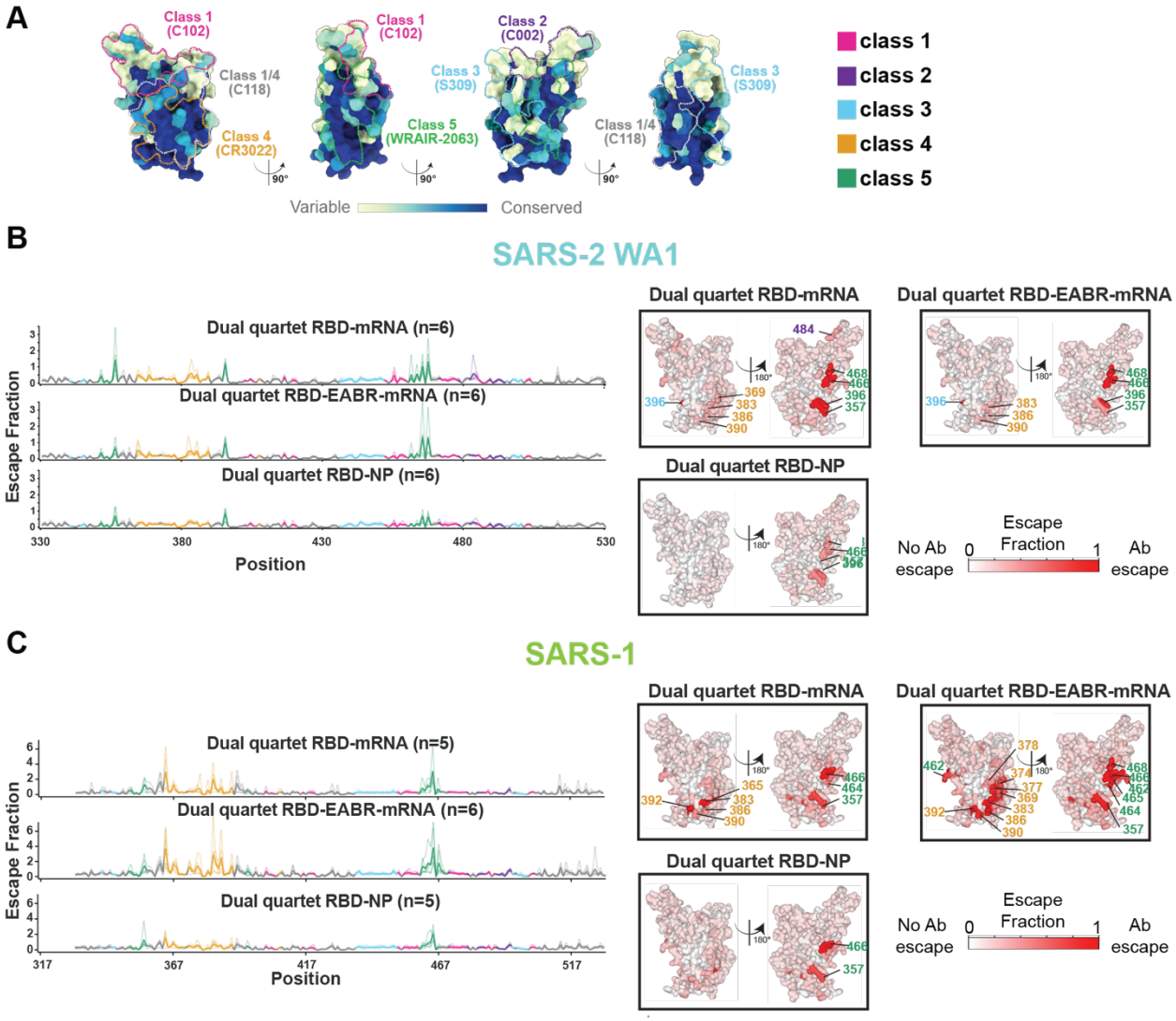

Figure 4. Dual quartet RBD-mRNA immunogens elicit Ab responses against conserved class 4 and class 5 RBD epitopes.

(A) Sequence conservation of 16 sarbecovirus RBDs calculated using ConSurf (Landau et al., 2005) shown on a surface representation of SARS-2 RBD (PDB 7BZ5). Class 1, 2, 3, 4, 1/4, and 5 anti-RBD Ab epitopes (Barnes et al., 2020; Cui et al., 2024; Jensen et al., 2023; Jette et al., 2021) are outlined in dots in different colors using information from representative structures of Abs bound to SARS-2 spike or RBD (C102: PDB 7K8M; C002: PDB 7K8T, S309: PDB 7JX3; CR3022: PDB 7LOP; C118: PDB 7RKV; WRAIR-2063: PDB 8EOO). (b,c) Left: Line plots for DMS results using a SARS-2 WA1 RBD library (B) and SARS-1 library (C) from the indicated number of mice immunized with the immunogens listed above each line plot. X-axis: RBD residue number. Y-axis: sum of the Ab escape of all mutations at a site (larger numbers = more Ab escape). Each line represents one antiserum with thick lines showing the average across the n = 5 or 6 sera in each group. Lines are colored according to RBD epitopes in panel A. Right: Average site-total Ab escape calculated for results from n = 5 or 6 serum samples for the indicated RBD yeast display libraries. Mice were immunized with the immunogens listed, and results were mapped to the highlighted residues on the surface of the SARS-2 WA1 RBD (PDB 6M0J). Gray indicates no escape; a gradient of red represents increasing degree of escape. Residue numbers show sites with the most escape with font colors representing different RBD epitopes (defined in panel A; class 1/4 residues are colored with fonts corresponding to class 1 or class 4 residues). The same data are shown in Table 1 and in Figs. S3 and S4 (line and logo plots for SARS-2 WA1 and SARS-1 RBD libraries, respectively).

Immunogen	Animal	WA1 DMS Profile						SARS-1 DMS Profile				
		class 1	class 2	class 3	class 4	class 5		class 1	class 2	class 3	class 4	class 5
Dual Quartet RBD-mRNA	9076											
Dual Quartet RBD-mRNA	9077											
Dual Quartet RBD-mRNA	9078											
Dual Quartet RBD-mRNA	9079											
Dual Quartet RBD-mRNA	9080											
Dual Quartet RBD-mRNA	9081											
Dual Quartet RBD-EABR-mRNA	9091											
Dual Quartet RBD-EABR-mRNA	9092											
Dual Quartet RBD-EABR-mRNA	9093											
Dual Quartet RBD-EABR-mRNA	9094											
Dual Quartet RBD-EABR-mRNA	9095											
Dual Quartet RBD-EABR-mRNA	9096											
Dual Quartet RBD-NP	9043											
Dual Quartet RBD-NP	9044											
Dual Quartet RBD-NP	9045											
Dual Quartet RBD-NP	9049											
Dual Quartet RBD-NP	9050											
Dual Quartet RBD-NP	9051											

Escape fraction

Polyclass	all classes <0.5	None	<0.5	Weak	0.5-1	Moderate	>1-2	Strong	>2

Table 1. Summary of DMS data showing elicitation of strong Ab responses against class 4 and class 5 RBD epitopes by dual quartet RBD-mRNA immunogens.

Results for individual mice are shown with ID numbers indicated. DMS was conducted using a SARS-2 WA1 RBD library (left) or a SARS-1 RBD library (right). DMS profiles were classified as polyclass, weak, moderate, or strong as indicated by the maximum escape fraction for any RBD position in each RBD epitope class. Colors and different designations for epitopes were assigned as indicated at the bottom (white entries for animals 9079 and 9045 indicate that no data were available). See also Fig. 4 and Figs. S3 and S4.

367
368 **mRNA-encoded dual quartet RBD immunogens elicit balanced IgG2a/IgG1 responses**
369 IgG subclasses induce distinct Fc effector functions, including opsonization, phagocytosis, and
370 Ab-dependent cell-mediated cytotoxicity, through differential binding of Fcs to Fc gamma
371 receptors (FcγRs) (Crescioli et al., 2025); e.g., mouse IgG1, IgG2a, and IgG2b bind the activating
372 receptor FcγR3 and the inhibitory receptor FcγR2b, IgG2a and IgG2b bind the activating receptor
373 FcγR4, and mouse IgG3 does not bind detectably to these FcγRs (Bruhns and Jonsson, 2015).
374 FcγR3 is more widely expressed than FcγR4, with FcγR4 mainly expressed on
375 monocytes/macrophages and neutrophils and FcγR3 found on those cells plus dendritic cells,
376 natural killer cells, basophils, mast cells, and eosinophils (Bruhns and Jonsson, 2015). In
377 immunized mice, IgG2a is associated with T_H1-type immune responses, effective activation of
378 complement, and protective interactions with FcγRs, which are critical functions for clearing
379 viruses (Hwang et al., 2021). IgG1, although usually efficient in neutralizing viruses, is associated
380 with T_H2-type responses thought to be less effective than T_H1 responses in combatting viruses
381 (Aleebrahim-Dehkordi et al., 2022).
382
383 We used systems serology (Ackerman et al., 2017) to evaluate IgG distributions elicited by mRNA
384 versus protein immunogens by comparing binding of IgG1, IgG2a, IgG2b, IgG3, FcγR2b-, FcγR3-
385 , or FcγR4-binding IgGs, and total IgG (IgGs isolated using a pan-IgG Ab) elicited by the five
386 immunogens to a panel of spike trimers and RBDs derived from SARS-2 variants and other
387 sarbecoviruses. Results show elicited responses from individual mice to each antigen (Fig. 5) and
388 geomean responses across antigens for each immunogen (Fig. S5).
389
390 Both dual quartet RBD-mRNA immunogens elicited high levels of IgG1 and IgG2a against
391 sarbecovirus spikes and RBDs, with somewhat higher levels of IgG2a than IgG1 (Fig. 5 and Fig.
392 S5), demonstrating a desirable mixture of IgGs for an anti-viral vaccine of induced T_H1 and T_H2
393 responses. In addition, the mRNA-based immunogens elicited significantly higher IgG2a and
394 FcγR4-binding IgG responses than the protein-based immunogens ($p<0.0001$) (Fig. S5). Dual
395 quartet RBD-NPs and dual quartet RBD-eVLPs elicited higher levels of IgG1 than IgG2a,
396 consistent with their administration with Addavax adjuvant, which enhances T_H2-biased immune
397 responses (Han et al., 2019). Dual quartet RBD-eVLPs also elicited significantly higher IgG2a
398 than dual quartet RBD-NPs ($p<0.0001$). Interestingly, dual quartet RBD-EABR-mRNA elicited
399 significantly higher IgG2b ($p<0.0001$), as well as FcγR3- ($p=0.0013$) and FcγR4- ($p=0.0021$)
400 binding IgGs, than dual quartet RBD-mRNA. Consistent with demonstrations of more limited
401 sarbecovirus recognition properties of Abs raised in response to homotypic RBD-NPs (Cohen et
402 al., 2021a; Cohen et al., 2024; Cohen et al., 2022; Fan et al., 2025b), SARS-2 RBD-eVLP elicited
403 IgGs mainly against SARS-2 and closely related RBDs (Fig. 5).
404
405 Thus, mRNA versions of dual RBD quartets elicit balanced IgG responses that broadly recognize
406 sarbecovirus antigens, arguing for their likely efficacy to protect against diverse sarbecoviruses.
407

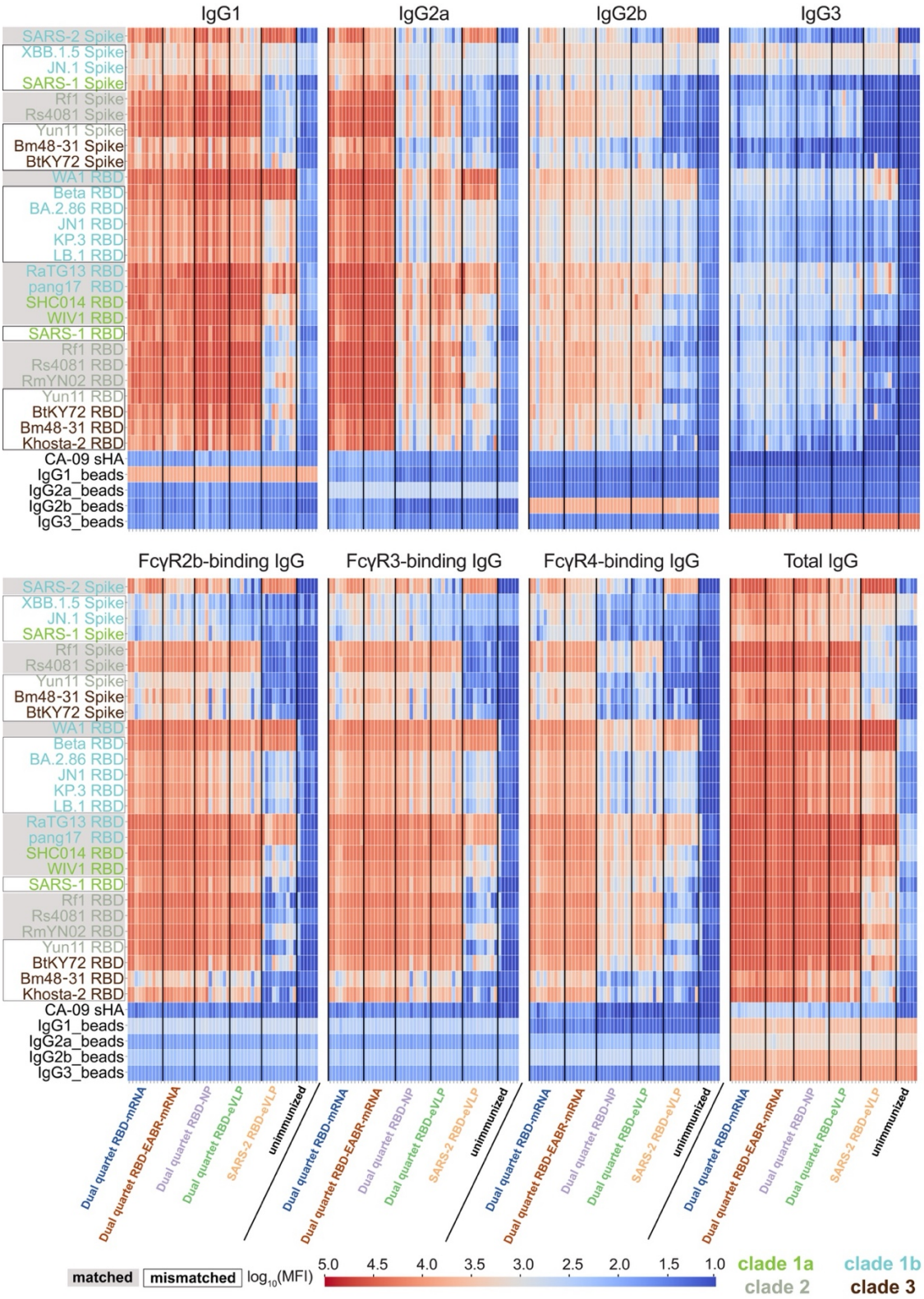

Figure 5. mRNA-encoded dual quartet RBD immunogens elicit balanced IgG subclass and potent FcγR-binding responses.

MFI = median fluorescent intensity. Binding of IgG1, IgG2a, IgG2b, IgG3, FcγR2b-binding IgGs, FcγR3-binding IgGs, FcγR4-binding IgGs, and total IgG to the indicated spikes, RBDs, or non-

414 sarbecovirus control proteins. Antigen names (y-axes) are colored according to spike or RBD
415 clades. Matched antigens are indicated with gray shading around the name, and mismatched
416 antigens are indicated with a black outline around the name. Each column represents binding data
417 from an individual mouse, and immunization cohorts are separated by a vertical black line. A
418 soluble influenza hemagglutinin trimer (CA-09 sHA) was used as a control to evaluate non-
419 specific binding. See also Fig. S5.
420
421 **Systems Serology-Polyclonal Epitope Mapping (SySPEM)**
422 To further explore potential differences in RBD recognition properties by different IgG subclasses
423 within polyclonal Ab samples, we combined systems serology with epitope mapping in a new
424 methodology we call Systems Serology-Polyclonal Epitope Mapping (SySPEM) (Fig. S6), by
425 analogy to Electron Microscopy-based Polyclonal Epitope Mapping (EMPEM) (Turner et al.,
426 2023). For epitope mapping by SySPEM, we created epitope knock-out (KO) mutants in the
427 SARS-2 WA1 RBD by introducing one or more potential N-linked glycosylation sites (PNGSs) to
428 direct addition of N-glycan(s) in RBD epitopes that are recognized by either class 1 and class 2,
429 class 2 only, class 3, class 1/4, class 4, or class 5 anti-RBD mAbs (Fig. S7 A). Addition of N-
430 glycan(s) at introduced PNGS(s) was verified by SDS-PAGE of purified RBD KO proteins, and
431 correct folding and epitope blocking were verified using a panel of control mAbs (Fig. S7, B and
432 C). We measured binding of total polyclonal IgG and IgG subsets to unmodified (wildtype; wt)
433 WA1 RBD and to each RBD KO mutant, defining a SySPEM score for an IgG sample/epitope
434 pair as [1.0 – (RBD KO binding / RBD wt binding) x 100]; thus, higher SySPEM scores indicate
435 increased binding by a particular IgG class to that epitope (Fig. S6). We present SySPEM results
436 in three formats to visualize epitope recognition across immunogens and Ab subclasses: (*i*) Median
437 SySPEM scores from individual mice divided into distinct RBD epitopes recognized by different
438 IgG classes with statistical comparisons between immunogen cohorts (Fig. 6). This comparison
439 highlights differences in epitope recognition across immunogen cohorts. (*ii*) Median SySPEM
440 scores for each IgG class within a given immunogen cohort with statistical comparisons between
441 targeted epitopes (Fig. S8). This shows the epitope distribution for a given immunogen/IgG class
442 pair, allowing for epitope profile comparisons between different immunogens, analogous to a
443 DMS profile (e.g., Fig. 4). (*iii*) Uniform Manifold Approximation and Projection (UMAP)
444 (McInnes et al., 2020) format to reduce the data set dimensions (Fig. 7). These figures provide
445 hierarchical views of the SySPEM data: statistical comparisons across immunogens (Fig. 6),
446 detailed within-cohort analyses (Fig. S8), and global similarity mapping of Ab recognition patterns
447 (Fig. 7).
448
449 SySPEM scores validated the mapping approach using RBD KO mutants by showing significantly
450 higher scores for total IgGs elicited by homotypic SARS-2 RBD-eVLPs than by other immunogens
451 against variable epitopes (class 1/class 2, class 2) and little to no targeting of more conserved
452 epitopes (class 4, class 1/4, class 5) (Fig. 6), as previously observed by DMS for homotypic SARS-
453 2 RBD-NPs (Cohen et al., 2022).
454
455 For IgG1, the mRNA- and protein-based dual quartet immunogens showed the highest class 5
456 SySPEM scores, with only dual quartet RBD-mRNA exhibiting a score that was not significantly
457 higher than that of homotypic SARS-2 RBD-eVLPs (Fig. 6). In addition, dual quartet RBD-eVLPs
458 and dual quartet RBD-EABR-mRNA exhibited class 4 and class 1/4 IgG1 SySPEM scores that
459 were significantly higher than respective scores for SARS-2 RBD-eVLPs. Similarly, for IgG2a,
460 the dual quartet immunogens all elicited significantly higher class 5 responses than homotypic
461 SARS-2 RBD-eVLP, with both dual quartet RBD-EABR-mRNA and dual quartet RBD-eVLP
462 featuring the highest class 5 SySPEM scores. Dual quartet RBD-EABR-mRNA, dual quartet RBD-

463 NP, and dual quartet RBD-eVLP also elicited higher class 4 SySPEM scores than SARS-2 RBD-
464 eVLP. Although not significant, dual quartet RBD-mRNA elicited a higher class 1/class 2
465 SySPEM score than dual quartet RBD-EABR-mRNA, and the opposite trend was observed for
466 class 5. These differences might explain the more potent SARS-2 D614G neutralization elicited
467 by dual quartet RBD-mRNA compared to dual quartet RBD-EABR-mRNA (Fig. 2 C), since class
468 1 and class 2 anti-RBD Abs are potent against SARS-2 WA1 (Barnes et al., 2020). However, the
469 combination of higher class 5 and lower class 1/class 2 responses elicited by the dual quartet RBD-
470 EABR-mRNA immunogen represents a more favorable epitope targeting profile for broad pan-
471 sarbecovirus vaccine efforts. For IgG2b and IgG3, SySPEM scores were more similar across the
472 different RBD epitope categories, although dual quartet RBD-eVLP showed significantly higher
473 class 4 and class 5 SySPEM scores than SARS-2 RBD-eVLP.
474
475 For total IgG, dual quartet RBD-EABR-mRNA and dual quartet RBD-NP showed higher class 5
476 SySPEM scores than SARS-2 RBD-eVLP, with dual quartet RBD-eVLP showing the highest
477 scores, and dual quartet RBD-mRNA showing class 5 scores that were not significantly higher
478 than those exhibited by SARS-2 RBD-eVLP (Fig. 6). Dual quartet RBD-EABR-mRNA exhibited
479 significantly higher class 4 and class 5 SySPEM scores for total IgG than dual quartet RBD-
480 mRNA, likely driven by the stronger class 4 and class 5 targeting by IgG2a for this comparison
481 (Fig. 6). Class 4 responses were higher for dual quartet RBD-EABR-mRNA, dual quartet RBD-
482 NP, and dual quartet RBD-eVLP all exhibiting significantly higher class 4 SySPEM scores than
483 SARS-2 RBD-eVLP, with dual quartet RBD-eVLP showing the highest class 4, 1/4, and 5 scores.
484
485 FcγR2b- and FcγR3-binding IgG SySPEM scores were similar across the RBD epitopes, with dual
486 quartet RBD-EABR-mRNA, dual quartet RBD-NP, and dual quartet RBD-eVLP all exhibiting
487 significantly higher class 5 SySPEM scores than SARS-2 RBD-eVLP (Fig. 6). Dual quartet RBD-
488 eVLP and, to a lesser extent, dual quartet RBD-EABR-mRNA exhibited higher class 4 SySPEM
489 scores than SARS-2 RBD-eVLPs. For FcγR4-binding IgGs, dual quartet RBD-EABR-mRNA,
490 dual quartet RBD-NP, and dual quartet RBD-eVLP showed significantly higher class 4 and class
491 5 SySPEM scores than SARS-2 RBD-eVLP.
492
493 To identify all epitopes recognized by sera elicited by a given immunogen, we displayed the
494 SySPEM results in a format in which SySPEM scores for recognition of individual RBD epitopes
495 by different IgG classes are shown (Fig. S8). These results highlight increased targeting of class 5
496 RBD epitopes by IgG1, IgG2a, IgG2b, and IgG3 subclasses elicited by the four dual quartet
497 immunogens, but not by homotypic SARS-2 RBD-eVLPs. Displaying the data in this format
498 showed that in some cases for a given immunogen, different IgG subclasses can exhibit distinct
499 epitope profiles, e.g., IgG1 and IgG2a from dual quartet EABR-mRNA sera, where IgG1 showed
500 higher class 1 and class 2 targeting than IgG2a, for which only class 5 targeting was high.
501
502 To visualize global patterns of epitope recognition between the different immunogens, we made
503 UMAPs (McInnes et al., 2020) to project epitope profiles into two- or three-dimensional plots (Fig.
504 7). For 2D UMAPs (Fig. 7, A-E), clusters of points indicate samples that behaved similarly across
505 all epitope knockouts, with ellipses indicating the spread of responses from each immunogen, and
506 centroid markers (indicated by an X) indicating the average epitope mapping profile for each
507 immunogen. When comparing IgG1 (Fig. 7 A), IgG2a (Fig. 7 B), IgG1, IgG2a, IgG2b, and IgG3
508 (Fig. 7 C), and total IgG (Fig. 7 D), epitope profiles for different immunogens showed similar
509 trends with SARS-2 RBD-eVLP clustering farthest from the four dual quartet immunogens, and
510 the dual quartet immunogens showing more overlap with each other. Dual quartet RBD-mRNA

511 mapped closer to SARS-2 RBD-eVLP in all cases (Fig. 7, A-E), as is especially apparent for IgG2a
512 (Fig. 7 B), total IgG (Fig. 7 D), and the FcγRs (Fig. 7 E). By contrast, dual quartet RBD-EABR-
513 mRNA clustered further away from SARS-2 RBD-eVLP and closer to dual quartet RBD-eVLP.
514 Dual quartet RBD-NP mapped similarly to dual quartet RBD-EABR-mRNA. To further assess
515 differences in epitope recognition between different immunogens, a three-dimensional UMAP plot
516 was generated using all data (Fig. 7 F). Trends in the 3D map were consistent with the 2D UMAPs
517 in that responses to the dual quartet immunogens were distinct from responses to SARS-2 RBD-
518 eVLP and responses to dual quartet RBD-EABR-mRNA tended to map between dual quartet
519 RBD-mRNA and the protein-based dual quartets, consistent with the EABR approach that
520 combines traditional mRNA- and protein-based vaccinations (Hoffmann et al., 2023). In addition,
521 finding that SySPEM scores for dual quartet RBD-mRNA overlapped more with scores for SARS-
522 2 RBD-eVLP than scores for the other dual quartet immunogens is consistent with more class
523 1/class 2 RBD epitope targeting by dual quartet RBD-mRNA and SARS-2 RBD-eVLP (Table 1).
524
525 Overall, the SySPEM studies confirmed targeting of more conserved RBD epitopes by the mRNA-
526 based dual quartet immunogens, particularly the EABR-modified version, indicating successful
527 conversion of the desirable properties of protein-based mosaic-8 immunogens. With detailed
528 analyses, however, we found distinct epitope profiles for IgG subclass and FcγR-binding IgGs:
529 i.e., the same antigens presented via different modalities (mRNA plus and minus EABR sequences
530 and protein antigens on NPs or eVLPs) showed divergent SySPEM epitope profiles. In addition,
531 SySPEM profiling of binding data rationalized differences in neutralization profiles when
532 comparing two similar immunogens presented differently (e.g., dual quartet RBD-EABR-mRNA
533 versus dual quartet RBD-mRNA).
534
535

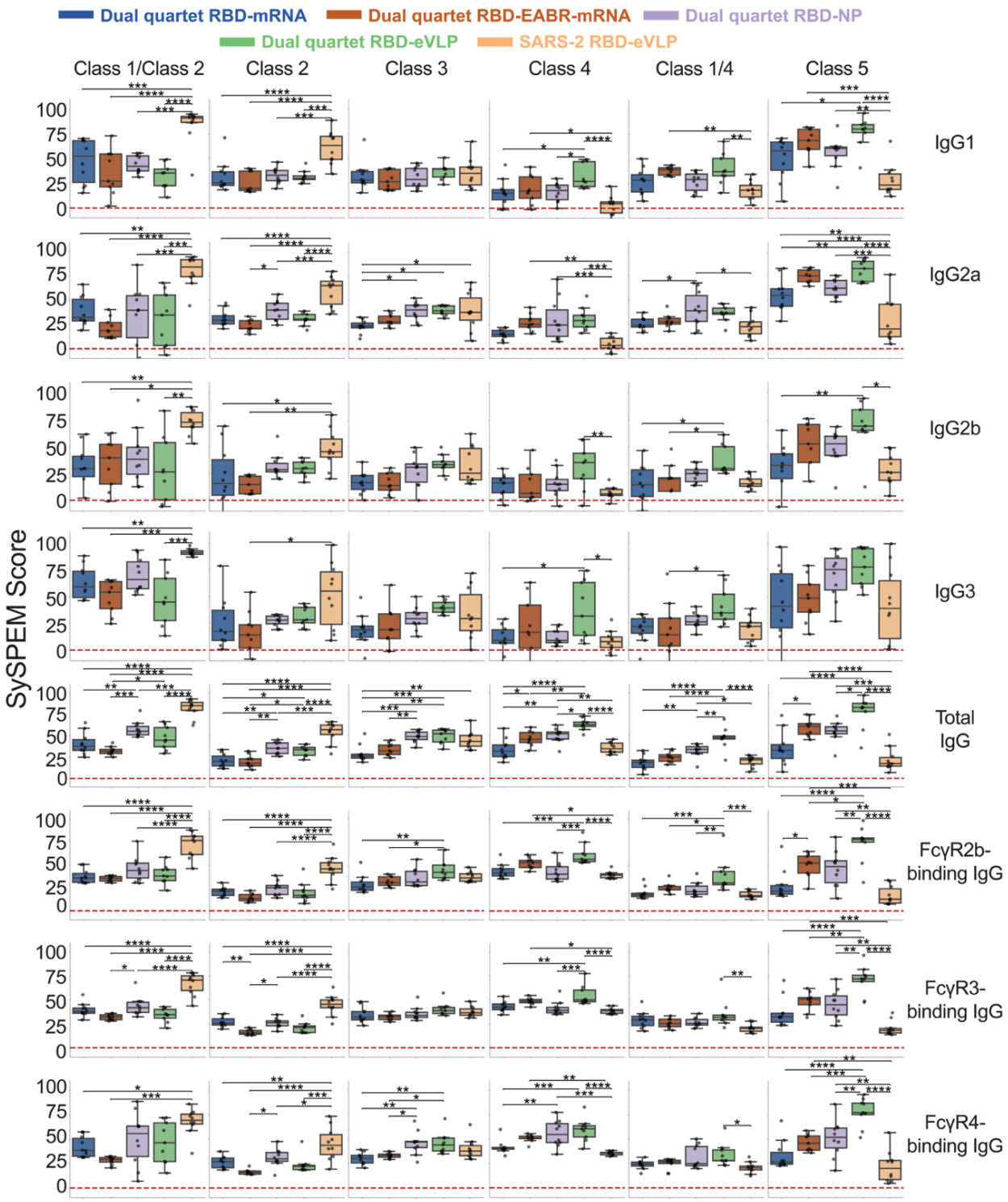

Figure 6. SySPEM score comparisons show differences in epitope recognition across immunogen cohorts.

SySPEM scores from individual mice were determined for RBD epitopes (columns) recognized by different IgG classes (rows, IgG subclass plus different FcγR-binding IgGs) with statistical comparisons between immunogen cohorts (colors). A SySPEM value of 0 indicates that none of the IgGs in that sample were affected by the glycan addition and therefore the sample did not contain IgGs that recognize that epitope, and a SySPEM value of 100 indicates that all IgGs in that

sample recognized that epitope (Fig. S6). A SySPEM value between 0 and 100 indicates the proportion of IgGs in a sample that recognized the epitope that was blocked by glycan addition in the RBD KO mutant. Box and whisker plots of SySPEM scores with individual data points representing one mouse are shown. Significant differences between cohorts were calculated using Tukey's HSD posthoc test and linked by vertical lines indicated by asterisks: $p<0.05$ = *, $p<0.01$ = **, $p<0.001$ = ***, $p<0.0001$ = ****. See also Fig. 7 and Fig. S8.

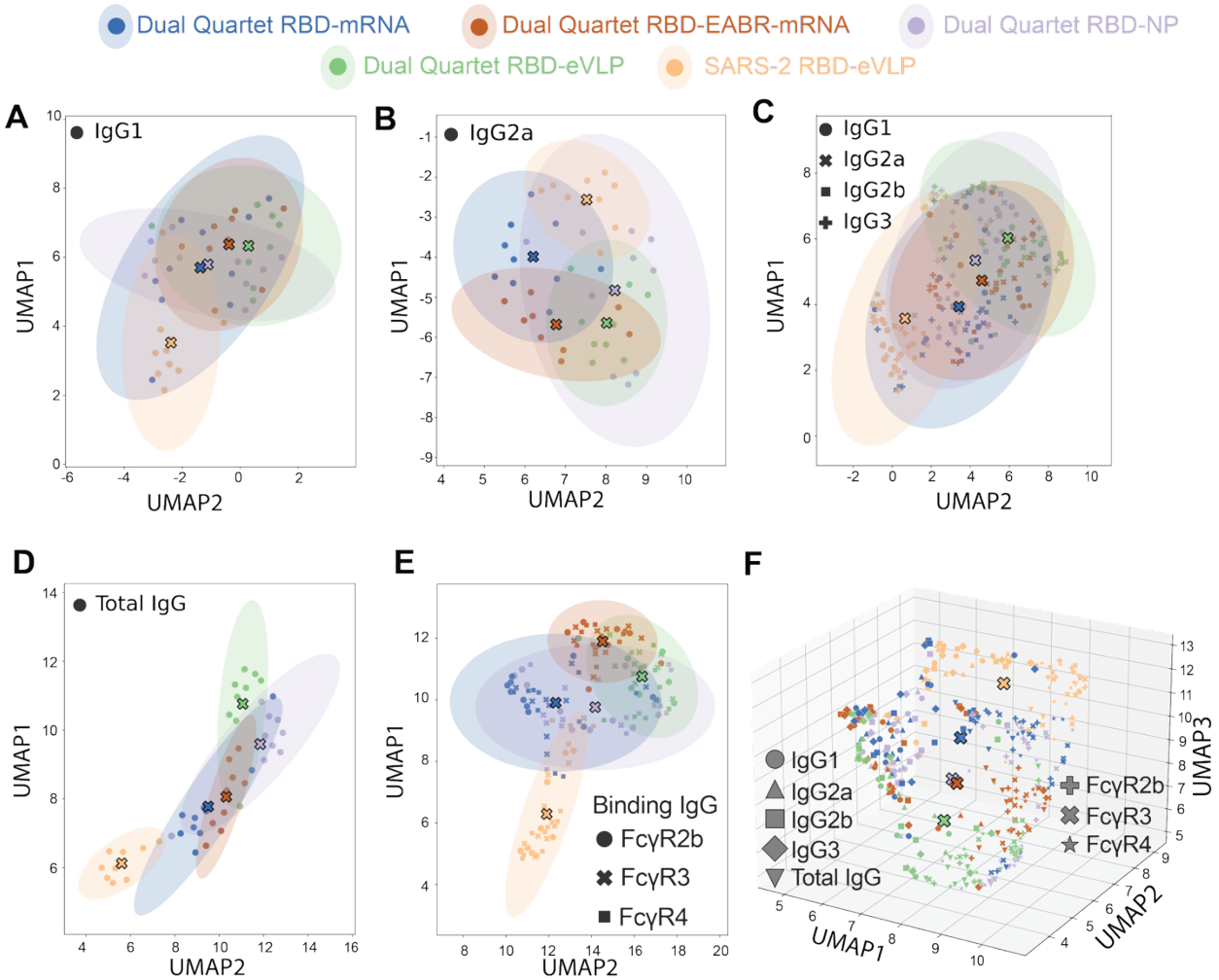

Figure 7. SySPEM UMAP analyses.
Uniform Manifold Approximation and Projection (UMAP) (McInnes et al., 2020) was used to project multi-dimensional SySPEM scores into two (panels A-E) or three (panel F) dimensions for (A) IgG1 (B) IgG2a, (C) IgG1, IgG2a, IgG2b, and IgG3, (D) Total IgG, (E) FcγR-binding IgGs, and (F) Total IgG, FcγR-binding IgGs, and IgG subclasses. Samples with similar Ab–epitope recognition profiles cluster together, with colored ellipses indicating the variance within each immunogen group and centroid markers (large Xs) showing the group mean. (F) Three-dimensional UMAP projection for all IgG subclasses and FcγR-binding IgGs with centroid markers (large Xs). See also Fig. 6, Figs. S6 and S8.

Discussion

565 mRNA-based COVID-19 vaccines have been critical for preventing severe disease and death after
566 SARS-2 infection (Wong and Mabbott, 2024), thereby helping keep the worldwide pandemic in
567 check. A recent modification of Moderna's mRNA-1273 vaccine involved changing the encoded
568 antigen from a SARS-2 spike trimer to a membrane-bound spike N-terminal domain and RBD
569 (Stewart-Jones et al., 2023). The new vaccine, mRNA-1283, exhibited equivalent or superior
570 induced immune responses compared to mRNA-1273 in mice (Stewart-Jones et al., 2023) and
571 humans (Chalkias et al., 2025), thus supporting further development of RBD-based COVID-19
572 and broader CoV vaccines.
573
574 We previously described protein-based RBD-NP immunogens that show promise as a pan-
575 sarbecovirus vaccine (Cohen et al., 2021a; Cohen et al., 2024; Cohen et al., 2022; Fan et al., 2022;
576 Fan et al., 2025b; Hills et al., 2024; Wang et al., 2025). However, manufacturing a protein-based
577 mosaic-8 NP vaccine presents challenges: mosaic-8 RBD-NP requires expression and purification
578 of nine protein components (eight RBDs and a NP) to generate a conjugated RBD-NP, which then
579 requires additional purification and characterization. mRNA vaccines offer the possibility of
580 simpler manufacturing (Pardi et al., 2018) but developing eight individual RBD constructs would
581 also be challenging, especially since mRNA delivery might not achieve co-display of all eight
582 RBDs on cell surfaces and/or eVLPs.
583
584 Here, we report an efficient approach to develop an mRNA-encoded version of a broadly cross-
585 reactive mosaic-8 RBD-NP vaccine. The new approach, inspired by protein-based dual quartet
586 RBD-NPs (Hills et al., 2024), involves genetically encoding sarbecovirus RBDs arranged as two
587 membrane-bound quartets, each comprising four tandemly arranged RBD ectodomains. RBD
588 quartets offer the opportunity for optimal Ab induction by displaying a greater number of RBDs
589 per transmembrane region compared with presentation of individual RBDs. The mRNA
590 immunogens described here display dual RBD quartets at cell surfaces (dual quartet RBD-mRNA)
591 or at both the surfaces of cells and secreted eVLPs (dual quartet RBD-EABR-mRNA) when an
592 EABR cytoplasmic domain sequence is included (Hoffmann et al., 2023). Our analyses showed
593 that dual quartet mRNA immunogens elicited equivalent or superior Ab responses, improved FcγR
594 binding of elicited Abs, and increased T cell responses compared with protein-based dual quartet
595 RBD-NPs. In addition, the dual quartet mRNA immunogens induced balanced T_H1/T_H2 responses,
596 thereby stimulating both cellular and humoral immune responses. Finally, of critical importance
597 for a potential pan-sarbecovirus vaccine, DMS showed that mRNA-based dual RBD quartet
598 immunogens induced Abs against conserved RBD epitopes, as required for a pan-sarbecovirus
599 vaccine and as observed for protein-based mosaic-8 RBD-NP immunogens (Cohen et al., 2021a;
600 Cohen et al., 2024; Cohen et al., 2022; Fan et al., 2022; Fan et al., 2025b; Hills et al., 2024; Wang
601 et al., 2025).
602
603 Despite eliciting high Ab binding titers against both SARS-2 variants and non-SARS-2
604 sarbecoviruses, neutralization titers for mosaic-8 immunogens (dual quartet RBD mRNAs, dual
605 quartet RBD-NPs, and dual quartet RBD-eVLPs) were lower against SARS-2 variants than against
606 zoonotic sarbecoviruses (Fig. 2 C, Fig. S2 B). However, we recently reported increased
607 neutralizing titers against hard-to-neutralize viruses including Omicron elicited by pulsatile release
608 of a single injection of mosaic-8 RBD-NPs using atomic layer deposition (ALD) compared with
609 bolus prime and boost injections of the same immunogen (Cohen et al., 2025). ALD is also an
610 effective delivery mechanism for mRNA vaccines (Coleman et al., 2025), offering the possibility
611 that increased neutralizing potencies would be observed for ALD formulations of mRNA-based
612 mosaic-8 immunogens. In addition, improved neutralization of SARS-2 variants might be achieved
613 by changing the RBD composition of mosaic-8 immunogens; e.g., a computationally-designed

614 mosaic-7 RBD-NP elicited stronger neutralizing and binding Ab responses than original mosaic-
615 8 RBD-NPs (Wang et al., 2025), and in independent studies of the immunogenicity of different
616 mosaic RBD immunogen compositions, we observed increased cross-reactive responses when we
617 removed the SARS-2 RBD from mosaic RBD immunogens (Cohen et al., 2024; Wang et al.,
618 2025). Thus, altering the composition of dual RBD quartets (e.g., adding an Omicron RBD to an
619 RBD quartet, adding clade 3 RBDs, and/or removing all SARS-2 RBDs) might improve
620 neutralization potencies against SARS-2 variants.
621
622 In the absence of neutralization, binding Ab responses can trigger immune responses to clear
623 infected cells through Fc-mediated effector functions (Paciello et al., 2024) and/or complement
624 activation (Abu-Humaidan et al., 2022), and binding Ab titers correlate with protection in humans
625 and animals vaccinated with COVID-19 mRNA vaccines (Corbett et al., 2021; Gilbert et al., 2022;
626 Goldblatt et al., 2022). Indeed, human mAbs that neutralized early SARS-2 strains but lost
627 neutralizing activity against SARS-2 Omicron variants retained Fc effector functions (Paciello et
628 al., 2024), and non-neutralizing human anti-RBD mAbs protected from a SARS-2 challenge in
629 animal models (Clark et al., 2024). In addition, T cell responses conferred protection from an
630 Omicron challenge in the absence of neutralizing Ab responses (Case et al., 2024), and CD4+ T
631 cells producing IFN-γ play critical roles in controlling SARS-CoV-2 infection independently of
632 Abs (Fumagalli et al., 2024). Thus, even in the absence of strong neutralizing Ab titers against
633 SARS-2 variants, the ability of mosaic-8 immunogens to elicit Abs that exhibit broad binding
634 across sarbecovirus RBDs and balanced T cell responses are desirable traits for a protective pan-
635 sarbecovirus vaccine.
636
637 For characterizing dual quartet immunogens, we describe a new systems serology technique,
638 SySPEM, that quantifies the degree of binding to individual epitopes on an antigen across IgG
639 subclasses and FcγR-binding IgGs, therefore allowing comparisons of epitope profiles elicited by
640 different immunogens that are not possible using traditional systems serology (Ackerman et al.,
641 2017). SySPEM allows higher throughput epitope mapping than, e.g., EMPEM (Turner et al.,
642 2023), but can deliver some of the same information while also delineating epitopes recognized
643 by different Ab classes. In contrast to epitope mapping competition ELISAs (Morris, 1996),
644 multiplexed SySPEM analyses use minimal sample volumes, do not rely on a mAb panel of known
645 epitopes, and provide more precise epitope definitions based on locations of introduced N-glycans.
646 SySPEM and DMS results are complementary, but SySPEM experiments are easier to execute,
647 require less material, and can allow quantitative comparisons between responses to distinct
648 epitopes for different immunogens and IgG classes. Also, the SySPEM results reported here
649 yielded mechanistic insights that were not revealed by DMS (e.g., quantifying differences in
650 responses to dual quartet RBD-mRNA and dual quartet RBD-EABR-mRNA). In addition, we used
651 SySPEM to show that the same antigen (dual quartet RBDs) delivered through mRNA- or protein-
652 based vaccine modalities elicited distinct IgG class-specific epitope profiles, suggesting that the
653 way an antigen is presented can impact its epitope recognition by the immune system.
654
655 SySPEM revealed potential advantages of the mRNA-EABR approach compared with a traditional
656 mRNA immunogen; e.g., although overall binding and neutralizing Ab titers were similar, the dual
657 quartet RBD-EABR-mRNA immunogen elicited stronger targeting of conserved class 4 and class
658 5 epitopes and weaker targeting of variable class 1/class 2 epitopes than dual quartet RBD-mRNA,
659 suggesting that addition of an EABR sequence could improve the effectiveness of an mRNA-
660 encoded dual quartet RBD pan-sarbecovirus vaccine. For example, immunogen presentation on
661 circulating eVLPs would promote wider antigen distribution to potentially engage more B cells
662 (Fan et al., 2025a; Hoffmann et al., 2023). Indeed, circulating RBD-eVLPs resulting from a dual

quartet RBD-EABR-mRNA immunogen offer similar advantages to a recently described mRNA-delivered RBD protein nanoparticle (Hendricks et al., 2025) but also encode membrane-bound antigens at cell surfaces that could trigger additional immune responses. eVLP budding in the EABR approach might facilitate continuous replenishment of the cell surface with antigen, potentially increasing overall levels of antigen being displayed. The small size of eVLPs compared with a cell also facilitates efficient internalization by antigen-presenting cells (Foged et al., 2005; Joshi et al., 2013; Kim et al., 2022; Zepeda-Cervantes et al., 2020), which could result in enhanced antigenic peptide presentation by class II MHC and activation of T follicular helper cells to promote B cell activation and germinal center formation (Fan et al., 2025a). Improvements for mRNA vaccines by including EABR appear to be general, as the EABR approach enhances vaccine-induced humoral responses against SARS-2 (Cohen et al., 2021a; Cohen et al., 2024; Cohen et al., 2022; Hills et al., 2024; Wang et al., 2025), RSV (Chai et al., 2025), and influenza (Zhang et al., 2025). We also showed that a bivalent Wuhan-Hu-1/BA.5 spike-EABR-mRNA booster elicited more balanced targeting of multiple RBD epitopes in pre-vaccinated mice than conventional monovalent and bivalent spike-mRNA boosters, which primarily targeted variable RBD epitopes (Fan et al., 2025a). Taken together, our findings suggest that EABR-mRNA delivery of mosaic and multivalent immunogens improves targeting of conserved epitopes to enhance Ab breadth.

Pan-sarbecovirus vaccine candidates evaluated in mice would ideally elicit broad-binding IgG2a and IgG2b subclasses that promote robust Fc effector functions (Bruhns and Jonsson, 2015; Crescioli et al., 2025) to target conserved epitopes and elicit IgGs that bind to activating Fc receptors (FcγR3 and FcγR4). Using SySPEM, we showed that dual RBD quartet immunogens, including the two mRNA-encoded versions, fulfill these criteria. There are many future potential applications for this new technology for design and evaluation of vaccines against a variety of viruses and other pathogens. For example, studies to establish correlates of protection of vaccines could include SySPEM evaluations to determine relative protective effects of epitope targeting by different classes of IgGs, thus establishing desirable parameters for future vaccine efforts. In addition, SySPEM can be used to determine whether some epitopes elicit IgGs with different potential Fc effector functions to inform immunogen design for eliciting optimal immune responses against a particular pathogen.

In summary, our data support advancement of dual quartet RBD-mRNA immunogens with an optimal RBD composition into clinical development as a next-generation booster vaccine to provide protection from emerging SARS-2 variants and to reduce the chances of a future zoonotic sarbecovirus spillover from causing a new epidemic or pandemic.

Methods

Membrane-bound RBD quartet constructs

Sequences of the extracellular domains of RBD quartets 4a and 4b were based on previously reported SpyTag-Quartet (Genbank PP13603) and SpyTag-Alternate Quartet (GenBank PP136032, Addgene plasmid ID 214728) sequences (Hills et al., 2024). mRNA constructs encoded a mouse Ig heavy chain signal peptide, codon-optimized RBD quartets 4a and 4b in which individual RBDs were separated by nine-residue Gly/Ser/Thr linkers followed by a five-residue Gly/Ser linker, the SARS-1 spike transmembrane domain, and a truncated spike cytoplasmic tail (McBride et al., 2007) (GenBank AAP13441.1, residues [1218-1235]). For RBD quartet 4a-EABR and 4b-EABR constructs, an endocytosis-preventing motif (EPM) (Hoffmann et al., 2023), four-residue Gly/Ser linker, and the EABR (Hoffmann et al., 2023) sequence were appended to the C-terminus. For in vitro assays, these constructs were cloned into the IVTpro T7 plasmid (Takara 6144), containing the immunogen open reading frame flanked by 5′ and 3′ untranslated regions (UTRs) and a genetically encoded poly(A) tail.

mRNA synthesis

For in vitro assays, IVTpro T7 plasmids encoding codon-optimized RBD quartet 4a, RBD quartet 4b, RBD quartet 4a-EABR, and RBD quartet 4b-EABR constructs were linearized by BspQI restriction digestion (NEB, R0712) and subsequently purified using the Zymo DNA Clean & Concentrator-25 kit (Zymo, D4034). mRNA was generated by in vitro transcription using the IVTpro™ T7 mRNA Synthesis Kit (Takara, 6144) following manufacturer's instructions, with the addition of the CleanCap Reagent AG (3' OMe) (TriLink, N-7413) and complete substitution of uridine with N1-Methylpseudouridine-5'-Triphosphate (TriLink, N-108; TriLink) to reduce immunogenicity (Hoffmann et al., 2023). mRNA was then purified by lithium chloride precipitation and an ethanol wash following standard protocols (Walker and Lorsch, 2013). Purified mRNA was resuspended in nuclease-free water and stored at –80 °C.

For mRNAs used for in vivo immunization studies, constructs were synthesized by RNAcore (https://www.houstonmethodist.org/research-cores/rnacore/) using proprietary manufacturing protocols including incorporation of the CleanCap Reagent AG (3' OMe) (TriLink, N-7413) and complete substitution of uridine with N1-Methylpseudouridine-5'-Triphosphate (TriLink, N-108). mRNAs were purified by oligo-dT affinity purification. To remove double-stranded RNA contaminants, mRNAs were further purified using a cellulose-based method as described (Baiersdorfer et al., 2019). In brief, cellulose fibers (0.2 g/mL) were equilibrated in chromatography buffer (10mM HEPES pH 7.2, 0.1 mM EDTA, 125 mM NaCl, 16% ethanol) and added to microcentrifuge spin columns. mRNA diluted in chromatography buffer was added and shaken vigorously at room temperature for 30 minutes. The flow-through containing single-stranded mRNA was collected and purified with a sodium acetate precipitation and an ethanol wash. The final purified mRNA was filtered through a 0.2 µm filter before storage at –80 °C (Baiersdorfer et al., 2019; Hoffmann et al., 2023).

mRNA transfections and flow cytometry

HEK293T cells were seeded at 1×10^6 cells per well in 6-well plates and incubated for 20 h before transfection with 2 µg of mRNA encoding RBD quartet 4a, RBD quartet 4b, and/or their EABR-fused counterparts (4a-EABR, 4b-EABR) using Lipofectamine™ MessengerMax™ (Thermo Fisher Scientific). Forty-eight hours post-transfection, supernatants were collected for eVLP purification by ultracentrifugation on a 20% sucrose cushion as described (Hoffmann et al., 2023).

748 Cells were gently detached, resuspended in PBS+ (PBS + 2 % FBS), and 100 µL aliquots were
749 taken for flow cytometry.

750 For the experiment shown in Fig. S1 A, cells were stained with the cross-reactive anti-RBD mAb
751 C118 (Jette et al., 2021; Robbiani et al., 2020) (2.5 µg/mL) for 30 min in the dark at room
752 temperature, washed, and subsequently stained with Alexa Fluor® 647-conjugated anti-human
753 IgG secondary Ab (Invitrogen, A21445; 1:4,000) for 15 min. After a final wash, cells were
754 resuspended in PBS+ and analyzed on an Attune NxT Flow Cytometer (Thermo Fisher).
755
756 For the experiment shown in Fig. S1 C, cells were either singly transfected or co-transfected with
757 combinations of RBD quartet 4a and 4b constructs and stained simultaneously with 2.5 µg/mL of
758 Alexa Fluor® 647-conjugated anti-Rs4081 RBD (Fan et al., 2025b) and Alexa Fluor® 488-
759 conjugated M8a-7 IgG (anti-WIV1 RBD) (Fan et al., 2022) mAbs for 30 min at room temperature
760 in the dark. After washing and resuspension, samples were analyzed on an Attune NxT Flow
761 Cytometer. Results were plotted using FlowJo 10.5.3 software.
762
763 **Production of dual quartet and SARS-2 RBD-eVLPs**
764 Dual quartet RBD-eVLP and SARS-2 RBD-eVLP samples were generated as described
765 (Hoffmann et al., 2023) by transfecting Expi293F cells (Gibco) cultured in Expi293F expression
766 media (Gibco) on an orbital shaker at 37°C and 8% CO_2. To generate dual quartet RBD-eVLPs,
767 DNA plasmids encoding RBD quartet 4a-EABR and RBD quartet 4b-EABR constructs were
768 mixed at a ratio of 1:1. 72 hours post-transfection, cells were centrifuged at 400 x g for 10 min,
769 supernatants were passed through a 0.45 µm syringe filter and concentrated using Amicon Ultra-
770 15 centrifugal filters with 100 kDa molecular weight cut-off (Millipore). eVLPs were purified by
771 ultracentrifugation at 50,000 rpm (135,000 x g) for 2 hours at 4°C using a TLA100.3 rotor and an
772 Optima™ TLX ultracentrifuge (Beckman Coulter) on a 20% w/v sucrose cushion. After removal
773 of supernatants by aspiration, pellets were re-suspended in 200 µL sterile PBS at 4°C overnight.
774 To remove residual debris, samples were centrifuged at 10,000 x g for 10 min, and supernatants
775 were collected. eVLPs were further purified by SEC using a Superose 6 Increase 10/300 column
776 (Cytiva) equilibrated with PBS. Peak fractions corresponding to eVLPs were combined and
777 concentrated to 250-500 µL in Amicon Ultra-4 centrifugal filters with 100 kDa molecular weight
778 cut-off. Samples were aliquoted and stored at -20°C.
779
780 The amount of SARS-2 RBD on SARS-2 RBD-eVLPs and the amount of dual quartet RBD on
781 dual quartet RBD-eVLPs were determined by quantitative Western blot analysis. Various dilutions
782 of SEC-purified eVLP samples and known amounts of either soluble SARS-2 RBD protein (Sino
783 Biological, 40591-V08H-B-20) or purified soluble SpyTagged dual quartet RBDs (SpyTagged
784 RBD quartets 4a and 4b were mixed at a ratio of 1:1) were separated by SDS-PAGE and transferred
785 to nitrocellulose membranes (0.45 µm) (Thermo Fisher Scientific, LC2001). Rabbit anti-SARS-2
786 S1 polyclonal IgG (Thermo Fisher Scientific, PA5-116916; 1:1,000) and HRP-conjugated goat
787 anti-rabbit IgG (Abcam, ab98467; 1:10,000) were used. Protein bands were visualized using ECL
788 Prime Western Blotting Detection Reagent (Cytiva, RPN2232). Band intensities of the respective
789 standards and eVLP sample dilutions were measured using ImageJ to determine RBD amounts.
790
791 **LNP encapsulation of mRNAs**
792 Purified dual quartet RBD-encoding mRNAs (RBD quartet 4a + RBD quartet 4b or RBD quartet
793 4a-EABR + RBD quartet 4b-EABR; 1:1 ratio) for in vivo studies were formulated in LNPs as
794 previously described (Pardi et al., 2015). 1,2-distearoyl-*sn*-glycero-3-phosphocholine, cholesterol,
795 a PEG lipid, and an ionizable cationic lipid dissolved in ethanol were rapidly mixed with an

796 aqueous acidic solution containing mRNA using an in-line mixer. The ionizable lipid and LNP
797 composition are described in the international patent application WO2017075531(2017). The post
798 in-line solution was dialyzed with PBS to remove the ethanol and displace the acidic solution. LNP
799 was measured for size (60-65 nm) and polydispersity (PDI < 0.075) by dynamic light scattering
800 (Malvern Nano ZS Zetasizer). Encapsulation efficiencies were >97% as measured by the Quant-
801 iT Ribogreen Assay (Invitrogen).
802
803 **Protein expression**
804 RBDs, RBD quartets, and soluble sarbecovirus spike-6P (Hsieh et al., 2020) (SARS-2 WA1 and
805 JN.1) or spike-2P (XBB.1.5, SARS-1, Rf1, Rs4091, Yun11, BM48-31, BtKY72) trimers were
806 expressed as described (Cohen et al., 2025; Cohen et al., 2022; Hills et al., 2024). Briefly, AviTag
807 and/or His-tagged proteins were purified from transiently-transfected Expi293F cells (Gibco) by
808 nickel affinity chromatography (HisTrap HP, Cytiva) and SEC (Superose 6 Increase 10/300,
809 Cytiva) (Barnes et al., 2020; Cohen et al., 2022; Wang et al., 2022). Fractions corresponding to
810 proteins of interest were pooled, concentrated, and stored at 4ºC. Biotinylated proteins were
811 generated as described (Tykvart et al., 2012) by co-transfection of AviTag/His-tagged spike and
812 RBD constructs with a plasmid encoding an endoplasmic reticulum-directed BirA enzyme (kind
813 gift from Michael Anaya, Caltech). The anti-Rs4081, anti-RmYN02, and anti-WIV1 RBD mAb
814 IgGs from Fig. S1 and the mAb IgGs and human ACE2-Fc protein shown in Fig. S7 C were
815 expressed, purified, and classified as recognizing the RBD epitopes as described (Barnes et al.,
816 2020; Fan et al., 2022; Fan et al., 2025b; Jette et al., 2021).
817
818 **Preparation of RBD-NPs**
819 For making dual quartet RBD-NPs, SpyCatcher003-mi3–C-Tag (Addgene 159995**)** subunits were
820 expressed in BL21 (DE3) *E. coli* (Agilent) as described (Rahikainen et al., 2021). SpyCatcher003-
821 mi3–C-Tag bacterial cell pellets were resuspended in 20 mL of 20 mM Tris-HCl pH 8.5, 300 mM
822 NaCl, supplemented with 0.1 mg/mL lysozyme, 1 mg/mL cOmplete mini EDTA-free protease
823 inhibitor (Roche), and 1.0 mM PMSF. After incubation at 4 °C for 45 min with end-over-end
824 mixing, an Ultrasonic Processor equipped with a microtip (Cole-Parmer) was used to perform
825 sonication on ice (four times for 60 s, 50% duty-cycle), and cell debris were cleared by
826 centrifugation (35,000 x g for 45 min at 4 °C). SpyCatcher003-mi3–C-Tag was purified by
827 ammonium sulfate precipitation (170 mg per mL of lysate) and resuspension, followed by SEC
828 using a HiPrep Sephacryl S-400 HR 16-60 column (GE Healthcare) equilibrated with PBS as
829 described (Rahikainen et al., 2021). Dual quartet RBD-NPs were generated by incubating purified
830 SpyCatcher003-mi3–C-Tag with a 1:1 molar ratio of purified SpyTagged RBD quartets at 4 ºC in
831 PBS.
832
833 **Immunization of mice**
834 Mouse procedures were approved by the Labcorp Institutional Animal Care and Use Committee.
835 Six- to 7-week-old female BALB/c mice from Charles River Laboratories (RRID:
836 IMSR_JAX:000664) were housed at Labcorp Drug Development, Denver, PA for immunizations.
837 All animals were healthy upon receipt and monitored during a 7-day acclimation period. Mice
838 were assigned randomly to experimental groups of 10 animals. Mouse cages were kept in a
839 climate-controlled room (68 - 79 ºC) at 50 ± 20% relative humidity and provided with Rodent Diet
840 #5001 (Purina Lab Diet) ad libitum.
841
842 Mice were immunized by intramuscular injection on days 0 and 28 with 1.5 or 0.5 µg dual quartet
843 RBD-mRNA, 1.5 or 0.5 µg dual quartet RBD-EABR-mRNA, 5 µg dual quartet RBD-NP, 5 µg
844 dual quartet RBD-eVLP, or 5 µg SARS-2 RBD-eVLP (based on RBD content for protein-based

845 immunogens). Prior to immunizations, dual quartet RBD-NP, dual quartet RBD-eVLP, and SARS-
846 2 RBD-eVLP immunogens were mixed with Addavax adjuvant (InvivoGen; 50% v/v). Serum
847 samples for ELISAs and neutralization assays were obtained on indicated days by retro-orbital
848 bleeding.
849
850 **ELISAs**
851 For eVLP sandwich ELISAs, 96-well high-binding plates (Corning, #9018) were coated overnight
852 at 4 °C with capture mAb (5 µg/mL in 0.1 M $NaHCO_3$, pH 9.8). Plates were blocked with 3% BSA
853 and 0.1% Tween-20 in TBS (TBS-T) for 30 min at room temperature, followed by addition of
854 serially diluted purified eVLP samples for 2 h. After washing, biotinylated detection Abs (5 µg/mL
855 in blocking buffer) were added for 2 h at room temperature. Plates were washed three times with
856 TBS-T, incubated with streptavidin-HRP (Abcam, 7403; 1:20,000) for 30 min, washed again, and
857 developed with 1-Step™ Ultra TMB-ELISA substrate solution (ThermoFisher). Reactions were
858 stopped with 1 N HCl and absorbance was measured at 450 nm.

859 For the ELISA in Fig. S1 B, plates were coated with either anti-Rs4081 (Fan et al., 2025b) or anti-
860 RmYN02 (Fan et al., 2025b) mAbs and detected with biotinylated C118 (Jette et al., 2021;
861 Robbiani et al., 2020). For the ELISA in Fig. S1 D, plates were coated with anti-WIV1 (Fan et al.,
862 2022) and detected with biotinylated anti-Rs4081 (Fan et al., 2025b).

863 For serum ELISAs, purified His-tagged RBD (2.5 µg/mL in 0.1 M sodium bicarbonate buffer pH
864 9.8) was coated onto Nunc® MaxiSorp™ 384-wellplates (Sigma) and incubated overnight at 4˚C.
865 After blocking with 3% bovine serum albumin (BSA), 0.1% Tween 20 in Tris-buffered saline
866 (TBS-T) for 1 hour at room temperature, blocking solution was removed by aspiration. For serum
867 ELISAs shown in Fig. 2 and Fig. S2, mouse serum (1:100 initial dilution) was serially diluted by
868 3.1-fold in TBS-T/3% BSA and then added to plates for 3 hours at room temperature, followed by
869 washing with TBS-T. Plates were then incubated for 1 hour with a 1:100,000 dilution of HRP-
870 conjugated anti-IgG secondary (goat anti-mouse IgG; Abcam; RRID: AB_955439), and plates
871 were washed with TBS-T. For mAb ELISAs shown in Fig. S7, purified mAbs were serially diluted
872 by 3.1-fold in TBS-T/3% BSA and then added to plates for 3 hours at room temperature, followed
873 by washing with TBS-T. Plates were then incubated for 1 hour with a 1:100,000 dilution of HRP-
874 conjugated anti-IgG secondary (goat anti-human IgG; SouthernBiotech 2014-05), and plates were
875 washed with TBS-T. SuperSignal™ ELISA Femto Substrate (ThermoFisher) was added as per
876 manufacturer's instructions, and luminescence was read at 425 nm. Data were collected in
877 duplicate and midpoint titers (ED_{50} values) were obtained using Graphpad Prism 10.5.0 assuming
878 a four-parameter dose-response curve fit.

879 **Pseudovirus neutralization assays**
880 Lentivirus-based pseudoviruses were produced in HEK293T cells (RRID:CVCL_0063) cultured
881 in Dulbecco's modified Eagle's medium (DMEM, Gibco) supplemented with 10% heat-
882 inactivated fetal bovine serum (FBS, Bio-Techne), 1% Penicillin/Streptomycin (Gibco), and 1%
883 L-Glutamine (Gibco) at 37 °C and 5% CO_2. HEK293T-hACE2 cells (RRID:CVCL_A7UK) (Starr
884 et al., 2021b) and high-hACE2 HEK-293T (kindly provided by Kenneth Matreyek, Case Western
885 Reserve University) target cells for neutralization assays were cultured in DMEM (Gibco)
886 supplemented with 10% heat-inactivated FBS (Bio-Techne), 5 mg/mL gentamicin (Sigma-
887 Aldrich), and 5 mg/mL blasticidin (Gibco) at 37 °C and 5% CO_2.
888
889 Lentiviral-based viruses were prepared as described (Crawford et al., 2020; Robbiani et al., 2020)
890 using genes encoding spike sequences lacking C-terminal residues in the cytoplasmic tail:

deletions of 21 residues (SARS-2 variants) or 19 residues (SARS-1, Khosta-2-SARS-1 chimera, BtKY72-SARS-1 chimera). BtKY72 (containing K493Y/T498W substitutions) and Khosta-2 pseudoviruses were made with chimeric spikes in which the RBD from SARS-1 (residues 323-501) was substituted with the RBD from BtKY72 K493Y/T498W (residues 327-503) or Khosta-2 (residues 324-500) as described. (Seifert et al., 2022). Cells were co-transfected with HIV-1-based lentiviral plasmids, a luciferase reporter gene, and a coronavirus spike construct, resulting in lentivirus-based pseudovirions expressing a sarbecovirus spike protein. Supernatants were harvested 48-72 hours post-transfection, filtered, and stored at -80 °C. Pseudovirus infectivity was determined by titration using HEK293T-hACE2 cells.

Prior to neutralization assays, serum from immunized mice was heat-inactivated at 56 ºC for 10 minutes. Heat-inactivated serum was three-fold serially diluted and incubated with pseudovirus for 1 hour at 37˚C, then the serum/virus mixture was added to HEK293T-hACE2 target cells or high-hACE2 HEK-293T cell line expressing hACE2 encoded with a consensus Kozak sequence (for SHC014 assays; kindly provided by Kenneth Matreyek, Case Western Reserve University) and incubated for 48 hours at 37ºC. After removing media, cells were lysed with Britelite Plus reagent (Revvity Health Sciences), and luciferase activity was measured as relative luminesce units (RLUs). Relative RLUs were normalized to RLUs from cells infected with pseudotyped virus in the absence of antiserum. Half-maximal inhibitory dilutions (ID_{50} values) were derived in AntibodyDatabase (West et al., 2013) using 4-parameter nonlinear regression.

ELISpot assays

Mice were euthanized on day 77 or 78, and spleens were collected and processed as described (Hoffmann et al., 2023). Briefly, spleens were homogenized using a gentleMACS Octo Dissociator (Miltenyi Biotec). Cells were passed through a 70 µm tissue screen, centrifuged at 1,500 rpm for 10 min, and resuspended in CTL-Test™ media (ImmunoSpot) containing 1% GlutaMAX™ supplement (Gibco). ELISpot assays were performed as described (Hoffmann et al., 2023). A SARS-CoV-2 spike PepMix™ pool of 315 peptides (15-mers with 11 amino acid overlap; JPT Peptide Technologies) was added to mouse IFNγ/IL4 double-color ELISpot plates (ImmunoSpot) at a concentration of 2 µg/mL, and 300,000 splenocytes were added per well. Plates were incubated at 37ºC for 24 hours. Biotinylated detection reagents, streptavidin-alkaline phosphatase (AP), and substrate reagents were added according to the manufacturer's guidelines. To stop the reactions, plates were gently rinsed with water three times. Plates were air-dried for two hours in a running laminar flow hood. Numbers of spots were quantified using a CTL ImmunoSpot S6 Universal-V Analyzer (Immunospot).

DMS Epitope Mapping

DMS experiments to map epitopes recognized by serum Abs were performed in biological duplicates using independent mutant RBD yeast libraries (WA1 (Starr et al., 2022) and SARS-1 (Starr et al., 2022) generously provided by Tyler Starr, University of Utah) as described (Cohen et al., 2022; Greaney et al., 2021d). Sera that had been heat inactivated for 30 min at 56 °C were incubated twice with 50 OD units of AWY101 yeast transformed with an empty vector in order to remove non-specific yeast-binding Abs. Expression of RBDs in libraries was induced in galactose-containing synthetic defined medium with Casamino acids (6.7g/L Yeast Nitrogen Base, 5.0 g/L Casamino acids, 1.065 g/L MES acid, and 2% w/v galactose plus 0.1% w/v dextrose). After 18 hours of induction, cells were washed twice and incubated with serum under conditions of gentle agitation for 1 hour at room temperature. Cells were labeled for 1 hour with a secondary Ab (1:200 Alexa Fluor-647-conjugated goat anti-mouse-IgG Fc-gamma, Jackson ImmunoResearch 115-605-008, RRID:AB_2338904) after washing twice.

940
941 Stained yeast cells were examined by fluorescence-activated cell sorting (FACS) using a Sony
942 SH800 cell sorter. Cells were gated to capture RBD mutants that showed reduced Ab binding
943 compared to a control. Cells were collected for each sample until ~5 x 10^6 RBD^+ cells were
944 processed, which corresponds to ~5 x 10^5- 1 x 10^6 RBD^+ Ab-escaped cells. These cells were grown
945 overnight in synthetic defined media (6.7 g/L Yeast Nitrogen Base, 5.0 g/L Casamino acids, 1.065
946 g/L MES acid, and 2% w/v dextrose, 100 U/mL penicillin, 100 µg/mL streptomycin) to expand
947 cells prior to plasmid extraction. DNA extraction and Illumina sequencing were done as described
948 (Hills et al., 2024) (raw sequencing data will be available on NCBI SRA). Escape fractions were
949 computed as described (Greaney et al., 2021d; Hills et al., 2024) using Swift DMS (Hills et al.,
950 2024) (available upon request). Escape scores were calculated using a filter to remove variants
951 with mutations that escaped binding because of poor expression, >1 amino acid mutation, or low
952 sequencing counts (Greaney et al., 2022; Hills et al., 2024).
953
954 Escape map visualizations (static line plots, logo plots, and structural depictions) were created
955 using Swift DMS (Hills et al., 2024). Line heights show the escape score for a particular amino
956 acid substitution, as described (Hills et al., 2024). In some visualizations, sites were categorized
957 based on RBD epitope region (Barnes et al., 2020; Cui et al., 2024; Jensen et al., 2023; Jette et al.,
958 2021): class 1 (pink; RBD residues 403, 405, 406, 417, 420, 421, 453, 455-460, 473-478, 486, 487,
959 489, 503, 504); class 2 (purple; residues 472, 479, 483-485, 490-495), class 3 (blue; residues 341,
960 345, 346, 437-450, 496, 498-501,), class 4 (orange; residues 365-390, 408), class 5 (green; residues
961 352-357, 396, 462-468). In structural depictions of DMS results, an RBD surface (PDB 6M0J)
962 was colored by the site-wise escape metric at each site, with red scaled at an escape fraction of 2.0.
963 Residues exhibiting the highest escape fractions were labeled with their residue number, which
964 was colored according to epitope class. Logo plot residues are colored according to RBD epitopes
965 within different classes as indicated on the legend.
966
967 We stratified DMS escape fraction values into four groups. Escape fractions for each RBD
968 substitution range from 0 (no cells with this substitution were sorted into the escape bin) to 1 (all
969 cells with this substitution were sorted into the serum Ab escape bin) (Greaney et al., 2021c). The
970 sum of escape fractions for all substitutions at a specific site is represented by the total escape peak
971 (Greaney et al., 2021c). DMS profiles with total escape peaks <0.5 at all sites were classified as
972 polyclass responses. DMS profiles with total escape peaks of 0.5 to 1, >1 to 2, or >2 at one or more
973 sites were classified as weak, moderate, or strong escape profiles, respectively, corresponding to
974 their RBD epitope (Table 1).
975
976 **Systems serology: Ab subclass and FcγR binding profiling**
977 Serum samples from immunized mice were analyzed in systems serology (Ackerman et al., 2017)
978 experiments as described (Cohen et al., 2025) using modifications of a Luminex assay to quantify
979 the levels of antigen-specific Ab subclasses and FcγR binding profiles, which allows for
980 simultaneous detection and quantification of multiple analytes (i.e., different antigens) in a single
981 sample (Brown et al., 2017). In brief, avidin (Sigma-Aldrich Catalog #: A9275-25MG) was
982 coupled by carbodiimide-NHS ester chemistry to magnetic Luminex microspheres (LuminexCorp)
983 using Sulfo-NHS (ThermoFisher™ Catalog number 24510) and 1-Ethyl-3-[3-
984 dimethylaminopropyl]carbodiimide hydrochloride (EDC) (ThermoFisher™ Catalog number
985 22980) according to the manufacturer's instructions. Microspheres were blocked for 30 min with
986 1% BSA in PBS pH 7.4 (assay buffer) and then washed twice with PBS. Microspheres were
987 incubated with biotinylated antigen (sarbecovirus spike trimer, RBD, or control antigen) at room

988 temperature for 2 hours in assay buffer followed by blocking with 10 µM biotin (Millipore Sigma,
989 Catalog B4501-100MG). Antigen-coupled microspheres were combined then incubated with heat-
990 inactivated serum samples for 1 hour at room temperature in 96-well plates (Corning) at 1:200 or
991 1:1000 dilutions. Unbound IgGs were removed by washing twice with 200 µL of assay buffer.
992 Total IgG was detected using a PE-conjugated secondary Ab recognizing mouse IgG (Southern
993 Biotech 1030-09S). For evaluating antigen binding by different IgG subclasses, secondary Abs
994 against mouse IgG subclasses (Southern Biotech 1070-09S, 1080-09S, 1090-09S, 1100-09S; PE-
995 coupled anti-IgG1, IgG2a, IgG2b, IgG3) were added at a 1:1000 dilution in assay buffer and
996 incubated for 1 hour with continuous shaking at room temperature. Excess primary and secondary
997 Abs were removed by washing twice with 200 µL of assay buffer. Beads were resuspended in 200
998 µL of assay buffer, run in duplicate, and flowed in single file past two lasers on a Luminex™
999 FLEXMAP 3D™ Instrument System. In a Luminex assay, each bead region is impregnated with
1000 a different ratio of fluorescent dyes such that bead region identity, and thereby antigen identity, is
1001 interrogated by the first laser. A second laser interrogates the signal of secondary Ab binding.
1002 Median fluorescence intensity (MFI) was calculated for all samples.
1003
1004 For evaluating FcγR-binding IgGs, soluble ectodomains of 6xHis-tagged FcγR2b, FcγR3, and
1005 FcγR4 were prepared as described (Cohen et al., 2025) and biotinylated by co-expression with
1006 BirA enzyme in Expi293T cells (Tykvart et al., 2012). Biotinylated FcγRs were purified on a
1007 HisTrap column (VWR) according to the manufacturer's instructions followed by SEC and then
1008 bound to PE-streptavidin (eBioscience). Labeled FcγRs were diluted 1:200 in assay buffer and
1009 incubated with serum-coated microspheres for 1 hour at room temperature with continuous
1010 shaking. Unbound primary and PE-labeled FcγR were removed as described for anti-IgG subclass
1011 secondary Abs. Beads were resuspended and run on a Luminex™ FLEXMAP 3D™ Instrument
1012 System to derive MFI values as described above.
1013
1014 Log_{10}-transformed heatmaps of antigen-specific IgG responses were generated using Python
1015 (v3.9.16) with the Pandas (v2.0.3), NumPy (v1.23.5), Matplotlib (v3.7.1), and Seaborn (v0.12.2)
1016 packages. A soluble influenza hemagglutinin trimer (listed as CA-09 HA in Fig. 5; expressed and
1017 purified as described (Cohen et al., 2021b)) was used as a control to evaluate non-specific binding.
1018
1019 **SySPEM**
1020 One or more potential N-linked glycosylation site sequons (Asn-x-Ser/Thr) (Lehle and Bause,
1021 1984) were introduced at solvent-exposed residue(s) within the class 1 and class 2, class 2, class
1022 3, class 4, class 1/4, or class 5 RBD epitopes (Barnes et al., 2020; Cui et al., 2024; Jensen et al.,
1023 2023; Jette et al., 2021) of the WA1 RBD (Fig. S7 A). Addition of N-glycan(s) was confirmed by
1024 SDS-PAGE as a shift in electrophoretic mobility to a higher apparent molecular weight (Fig. S7
1025 B). Proper folding of RBD KO mutants and expected effects of added N-glycans were verified by
1026 assaying the binding of characterized mAbs or a human ACE2-Fc construct (Jette et al., 2021) by
1027 ELISA (Fig. S7 C). Binding of serum subsets to RBD wt and RBD KO proteins was measured
1028 using a Luminex multiplexed bead-based immunoassay as described above. The SySPEM score
1029 for each IgG sample/epitope pair was calculated as [1.0 – (RBD KO binding / RBD wt binding) x
1030 100]. SySPEM scores range from limits of 100 (none of the IgGs in the sample bound to the RBD
1031 KO; i.e., all of the IgGs recognize the epitope that was targeted by the glycan addition) to 0 (all of
1032 the IgGs in the sample bound to the RBD KO; i.e., none of the IgGs recognize the epitope that was
1033 targeted by the glycan addition) (Fig. S6). Python (v3.9.16) with the Pandas (v2.0.3), NumPy
1034 (v1.23.5), Matplotlib (v3.7.1), and Seaborn (v0.12.2) packages were used for box and whisker
1035 plots of SySPEM data. For UMAP visualizations in Fig. 7, SySPEM scores of each serum sample

were organized into a feature matrix where each column contains an epitope class SySPEM score, and each row corresponds to an individual sample. Features were standardized using the standard scalar function on sckit-learn 1.4.2. UMAP was then performed with umap-learn (0.5.9.post2) on the standardized matrix. UMAP parameters: the nearest neighbors (n-neighbors) parameter was set to 12 and minimum distance (min-dist) was set to 0.25 to preserve the best local and global structures on the UMAP plot. Seaborn (v0.12.2) was used to plot resulting UMAPs.

Quantification and statistical analyses

We used pairwise comparisons, a method to evaluate sets of mean binding titers against individual viral strains for different immunization cohorts, as described previously (Cohen et al., 2024) to determine if results from different immunized cohorts were significantly different from each other. For ELISAs and neutralizations (Fig. 2), we used analysis of variance (ANOVA) followed by Tukey's multiple comparison post hoc tests with the Geisser-Greenhouse correction, with pairing by viral strain, of ED_{50}s/ID_{50}s (converted to $\log_{10}$ scale) calculated using GraphPad Prism 10.5.0 to identify statistically significant titer differences between immunized groups for ELISAs. For comparisons of neutralizing titers by strain (Fig. S2), statistically significant titer differences between immunized groups for each given strain were determined using unpaired t test calculated using GraphPad Prism 10.5.0. For ELISpot assays, statistically significant differences between immunized cohorts were calculated using ordinary one-way ANOVA followed by Tukey's multiple comparison test using GraphPad Prism.

For statistical analysis of systems serology results, responses were aggregated by computing the geometric mean (geomean) across replicate samples for each immunogen-antigen combination. Log_{10}-transformed geomeans were compared across immunogen groups using Tukey's multiple comparison post hoc tests with the Geisser-Greenhouse correction, with pairing by viral strain calculated using GraphPad Prism 10.5.0. Box-and-whisker plots were generated for each IgG subclass or FcγR-binding IgG, displaying individual antigen-level geomeans per immunogen. Python (v3.9.16) with statsmodels (v0.14.4) packages were used for SySPEM Tukey's HSD posthoc statistical analyses. Statistical significance was annotated using brackets and asterisk notation ($p < 0.05$ *, $p < 0.01$ **, $p < 0.001$ ***, $p < 0.0001$ ****).

Materials, data, and code availability

DMS raw sequencing data is available on the NCBI SRA under BioProject PRJNA1067836, BioSample SAMN52937385. SySPEM scores for each IgG sample/epitope pair will be made publicly available upon publication. Materials are available upon request to corresponding authors with a signed material transfer agreement, and other information required to analyze the data in this paper is available from the lead contacts upon request. Code used for data processing and visualization of DMS, systems serology, and SySPEM results is available upon request. The work is licensed under a Creative Commons Attribution 4.0 International (CC BY 4.0) license, which permits unrestricted use, distribution, and reproduction in any medium, provided the original work is properly cited. To view a copy of this license, visit https://creativecommons.org/licenses/by/4.0/. This license does not apply to figures/photos/artwork or other content included in the article that is credited to a third party; obtain authorization from the rights holder before using such material.

Acknowledgements

We thank Annie Rorick, Han Gao, and Priyanthi Gnanapragasam for experimental assistance, Jesse Bloom (Fred Hutchinson Cancer Research Center) and Tyler Starr (University of Utah) for RBD libraries, Ryan McNamara and Galit Alter (Ragon Institute) for help with Systems Serology experiments, Jost Vielmetter, Luisa Segovia, Alyssa Player, Annie Lam, and the Caltech Beckman

Institute Protein Expression Center for protein production, Igor Antoshechkin and the Caltech Millard and Muriel Jacobs Genetics and Genomics Laboratory for Illumina sequencing, Michael Anaya for help with Luminex experiments, Dom Aylard, Katie Lippert, and the Gladstone Flow Cytometry Core for help with flow cytometry, and Anthony West and Ying Tam (Acuitas) for critical reading of the manuscript.

Funding Declaration

These studies were funded by Wellcome Leap (P.J.B.), the National Institutes of Health P01-AI165075 (P.J.B.), DP5OD033362 (M.A.G.H.), and 1K99AI185267 (A.A.C.), the Medical Research Council (MRC grant no. MR/Y011910/1 to M.R.H.), the Merkin Institute for Translational Research (Caltech) (P.J.B.), and the James B. Pendleton Charitable Trust that supports the Gladstone Flow Cytometry Core. This manuscript is the result of funding in whole or in part by the National Institutes of Health (NIH). It is subject to the NIH Public Access Policy. Through acceptance of this federal funding, NIH has been given a right to make this manuscript publicly available in PubMed Central upon the Official Date of Publication, as defined by NIH.

Author Contributions

Conceptualization: A.A.C., J.R.K., R.A.H., M.R.H., M.A.G.H., P.J.B.; Methodology: A.A.C., M.A.G.H.; Software: A.A.C.; Investigation: A.A.C., J.R.K., LM, IM, A.-C.P.F., K.-M.A.D., HES, M.A.G.H.; Resources: R.A.H., W.J.M., P.J.C.L.; Writing – original draft: A.A.C., J.R.K., K.-M.A.D., M.A.G.H., P.J.B.; Writing – review and editing: A.A.C., J.R.K., K.-M.A.D., R.A.H., M.R.H., M.A.G.H., P.J.B.; Visualization: A.A.C., J.R.K., K.-M.A.D., M.A.G.H., P.J.B.; Supervision: M.R.H., M.A.G.H., P.J.B.; Funding: M.A.G.H., P.J.B..

Competing Interests

P.J.B. and A.A.C. are inventors on a US patent application (17/523,813) filed by the California Institute of Technology that covers mosaic RBD-NPs. M.A.G.H. and P.J.B. are inventors on a patent application (US17/835,751; international: PCT/US2022/032702) filed by the California Institute of Technology that covers the EABR technology. M.R.H. is an inventor on patents on spontaneous amide bond formation (EP2534484 and UK Intellectual Property Office 1706430.4) and a SpyBiotech co-founder and shareholder. P.J.B., M.A.G.H., A.A.C., J.R.K., K-M.A.D., R.A.H., and M.R.H. are co-inventors on a provisional US patent application filed by the California Institute of Technology that covers dual quartet mRNA immunogens. P.J.B. is a scientific advisor for Vaccine Company, Inc. M.A.G.H. is a scientific consultant for Vaccine Company, Inc. W.J.M. and P.J.C.L. are employees of Acuitas Therapeutics, a company developing LNP delivery technology; P.J.C.L. holds equity in Acuitas Therapeutics.

1121 **Literature cited**
1122

1123 Abu-Humaidan, A.H.A., F.M. Ahmad, D. Awajan, R.F. Jarrar, and N. Alaridah. 2022. Anti-
1124 SARS-Cov-2 S-RBD IgG Formed after BNT162b2 Vaccination Can Bind C1q and
1125 Activate Complement. *J Immunol Res* 2022:7263740.
1126 Ackerman, M.E., D.H. Barouch, and G. Alter. 2017. Systems serology for evaluation of HIV
1127 vaccine trials. *Immunol Rev* 275:262–270.
1128 Aleebrahim-Dehkordi, E., B. Molavi, M. Mokhtari, N. Deravi, M. Fathi, T. Fazel, M.
1129 Mohebalizadeh, P. Koochaki, P. Shobeiri, and A. Hasanpour-Dehkordi. 2022. T helper
1130 type (Th1/Th2) responses to SARS-CoV-2 and influenza A (H1N1) virus: From
1131 cytokines produced to immune responses. *Transplant Immunology* 70:
1132 Andersen, K.G., A. Rambaut, W.I. Lipkin, E.C. Holmes, and R.F. Garry. 2020. The proximal
1133 origin of SARS-CoV-2. *Nature Medicine* 26:450–452.
1134 Baiersdorfer, M., G. Boros, H. Muramatsu, A. Mahiny, I. Vlatkovic, U. Sahin, and K. Kariko.
1135 2019. A Facile Method for the Removal of dsRNA Contaminant from In Vitro-
1136 Transcribed mRNA. *Mol Ther Nucleic Acids* 15:26–35.
1137 Bangaru, S., A.M. Jackson, J. Copps, M.L. Fernandez-Quintero, J.L. Torres, S.T. Richey, B.
1138 Nogal, L.M. Sewall, A. Torrents de la Pena, A. Rehman, M. Guebre-Xabier, B. Girard,
1139 R. Das, K.S. Corbett-Helaire, R.A. Seder, B.S. Graham, D.K. Edwards, N. Patel, G.
1140 Smith, and A.B. Ward. 2025. Structural serology of polyclonal antibody responses to
1141 mRNA-1273 and NVX-CoV2373 COVID-19 vaccines. *Cell reports* 44:115986.
1142 Barnes, C.O., C.A. Jette, M.E. Abernathy, K.-M.A. Dam, S.R. Esswein, H.B. Gristick, A.G.
1143 Malyutin, N.G. Sharaf, K.E. Huey-Tubman, Y.E. Lee, D.F. Robbiani, M.C.
1144 Nussenzweig, A.P. West, and P.J. Bjorkman. 2020. SARS-CoV-2 neutralizing antibody
1145 structures inform therapeutic strategies. *Nature* 588:682–687.
1146 Brown, E.P., K.G. Dowell, A.W. Boesch, E. Normandin, A.E. Mahan, T. Chu, D.H. Barouch, C.
1147 Bailey-Kellogg, G. Alter, and M.E. Ackerman. 2017. Multiplexed Fc array for evaluation
1148 of antigen-specific antibody effector profiles. *J Immunol Methods* 443:33–44.
1149 Bruhns, P., and F. Jonsson. 2015. Mouse and human FcR effector functions. *Immunol Rev*
1150 268:25–51.
1151 Bruun, T.U.J., A.C. Andersson, S.J. Draper, and M. Howarth. 2018. Engineering a Rugged
1152 Nanoscaffold To Enhance Plug-and-Display Vaccination. *ACS Nano* 12:8855–8866.
1153 Case, J.B., S. Sanapala, C. Dillen, V. Rhodes, C. Zmasek, T.M. Chicz, C.E. Switzer, S.M.
1154 Scheaffer, G. Georgiev, C. Jacob-Dolan, B.M. Hauser, D.C.C. Dos Anjos, L.J. Adams, N.
1155 Soudani, C.Y. Liang, B. Ying, R.P. McNamara, R.H. Scheuermann, A.C.M. Boon, D.H.
1156 Fremont, S.P.J. Whelan, A.G. Schmidt, A. Sette, A. Grifoni, M.B. Frieman, and M.S.
1157 Diamond. 2024. A trivalent mucosal vaccine encoding phylogenetically inferred ancestral
1158 RBD sequences confers pan-Sarbecovirus protection in mice. *Cell Host Microbe*
1159 32:2131–2147 e2138.
1160 Chai, P., Y. Shi, X. Li, M. Yang, X. Liu, M. Liu, J. Yu, X. Yin, D. Li, K. Li, X. Kong, Q. Zhang,
1161 H. Wang, X. Sun, J. Li, L. Li, D. Li, L. Pang, X. Lu, and Z. Duan. 2025. Improved
1162 mRNA-based RSV vaccine with PreF forming enveloped virus-like particles. *NPJ*
1163 *Vaccines* 10:152.
1164 Chalkias, S., P. Dennis, D. Petersen, K. Radhakrishnan, L. Vaughan, R. Handforth, A. Rossi, R.
1165 Wahid, D.K. Edwards, J. Feng, W. Deng, H. Zhou, E. De Windt, V. Urdaneta, Y. Paila,
1166 B. Girard, S.N. Faust, S.R. Walsh, C.A. Cosgrove, J. Miller, and R. Das. 2025. Efficacy,
1167 immunogenicity, and safety of a next-generation mRNA-1283 COVID-19 vaccine
1168 compared with the mRNA-1273 vaccine (NextCOVE): results from a phase 3,
1169 randomised, observer-blind, active-controlled trial. *Lancet Infect Dis*

1170 Clark, J.J., I. Hoxie, D.C. Adelsberg, I.A. Sapse, R. Andreata-Santos, J.S. Yong, F. Amanat, J.
1171 Tcheou, A. Raskin, G. Singh, I. Gonzalez-Dominguez, J.E. Edgar, S. Bournazos, W. Sun,
1172 J.M. Carreno, V. Simon, A.H. Ellebedy, G. Bajic, and F. Krammer. 2024. Protective
1173 effect and molecular mechanisms of human non-neutralizing cross-reactive spike
1174 antibodies elicited by SARS-CoV-2 mRNA vaccination. *Cell reports* 43:114922.
1175 Cohen, A.A., P.N.P. Gnanapragasam, Y.E. Lee, P.R. Hoffman, S. Ou, L.M. Kakutani, J.R.
1176 Keeffe, H.J. Wu, M. Howarth, A.P. West, C.O. Barnes, M.C. Nussenzweig, and P.J.
1177 Bjorkman. 2021a. Mosaic nanoparticles elicit cross-reactive immune responses to
1178 zoonotic coronaviruses in mice. *Science* 371:735–741.
1179 Cohen, A.A., J.R. Keeffe, A.V. Rorick, S. Rho, A.-C. Priso Fils, L. Manasyan, H. Gao, P.N.P.
1180 Gnanapragasam, H.H. Funke, T.W. Randolph, R.L. Garcea, and P.J. Bjorkman. 2025.
1181 Broad anti-sarbecovirus responses elicited by a single administration of mosaic-8 RBD-
1182 nanoparticle vaccine prepared using atomic layer deposition. *iScience*
1183 Cohen, A.A., J.R. Keeffe, A. Schiepers, S.E. Dross, A.J. Greaney, A.V. Rorick, H. Gao, P.N.P.
1184 Gnanapragasam, C. Fan, A.P. West, Jr., A.I. Ramsingh, J.H. Erasmus, J.D. Pata, H.
1185 Muramatsu, N. Pardi, P.J.C. Lin, S. Baxter, R. Cruz, M. Quintanar-Audelo, E. Robb, C.
1186 Serrano-Amatriain, L. Magneschi, I.G. Fotheringham, D.H. Fuller, G.D. Victora, and P.J.
1187 Bjorkman. 2024. Mosaic sarbecovirus nanoparticles elicit cross-reactive responses in pre-
1188 vaccinated animals. *Cell* 187:5554–5571 e5519.
1189 Cohen, A.A., N. van Doremalen, A.J. Greaney, H. Andersen, A. Sharma, T.N. Starr, J.R. Keeffe,
1190 C. Fan, J.E. Schulz, P.N.P. Gnanapragasam, L.M. Kakutani, A.P. West, Jr., G. Saturday,
1191 Y.E. Lee, H. Gao, C.A. Jette, M.G. Lewis, T.K. Tan, A.R. Townsend, J.D. Bloom, V.J.
1192 Munster, and P.J. Bjorkman. 2022. Mosaic RBD nanoparticles protect against challenge
1193 by diverse sarbecoviruses in animal models. *Science* 377:eabq0839.
1194 Cohen, A.A., Z. Yang, P.N.P. Gnanapragasam, S. Ou, K.A. Dam, H. Wang, and P.J. Bjorkman.
1195 2021b. Construction, characterization, and immunization of nanoparticles that display a
1196 diverse array of influenza HA trimers. *PLoS One* 16:e0247963.
1197 Coleman, H.J., A. Rauch, E. Langsfeld, K. Anderson, U. Parlikar, H.H. Funke, R.L. Garcea, and
1198 T.W. Randolph. 2025. Lipid-free, thermostable mRNA vaccines prepared using atomic
1199 layer deposition. *J Pharm Sci* 104066.
1200 Corbett, K.S., D.K. Edwards, S.R. Leist, O.M. Abiona, S. Boyoglu-Barnum, R.A. Gillespie, S.
1201 Himansu, A. Schafer, C.T. Ziwawo, A.T. DiPiazza, K.H. Dinnon, S.M. Elbashir, C.A.
1202 Shaw, A. Woods, E.J. Fritch, D.R. Martinez, K.W. Bock, M. Minai, B.M. Nagata, G.B.
1203 Hutchinson, K. Wu, C. Henry, K. Bahl, D. Garcia-Dominguez, L. Ma, I. Renzi, W.P.
1204 Kong, S.D. Schmidt, L. Wang, Y. Zhang, E. Phung, L.A. Chang, R.J. Loomis, N.E.
1205 Altaras, E. Narayanan, M. Metkar, V. Presnyak, C. Liu, M.K. Louder, W. Shi, K. Leung,
1206 E.S. Yang, A. West, K.L. Gully, L.J. Stevens, N. Wang, D. Wrapp, N.A. Doria-Rose, G.
1207 Stewart-Jones, H. Bennett, G.S. Alvarado, M.C. Nason, T.J. Ruckwardt, J.S. McLellan,
1208 M.R. Denison, J.D. Chappell, I.N. Moore, K.M. Morabito, J.R. Mascola, R.S. Baric, A.
1209 Carfi, and B.S. Graham. 2020. SARS-CoV-2 mRNA vaccine design enabled by prototype
1210 pathogen preparedness. *Nature* 586:567–571.
1211 Corbett, K.S., M.C. Nason, B. Flach, M. Gagne, S. O'Connell, T.S. Johnston, S.N. Shah, V.V.
1212 Edara, K. Floyd, L. Lai, C. McDanal, J.R. Francica, B. Flynn, K. Wu, A. Choi, M. Koch,
1213 O.M. Abiona, A.P. Werner, J.I. Moliva, S.F. Andrew, M.M. Donaldson, J. Fintzi, D.R.
1214 Flebbe, E. Lamb, A.T. Noe, S.T. Nurmukhambetova, S.J. Provost, A. Cook, A. Dodson,
1215 A. Faudree, J. Greenhouse, S. Kar, L. Pessaint, M. Porto, K. Steingrebe, D. Valentin, S.
1216 Zouantcha, K.W. Bock, M. Minai, B.M. Nagata, R. van de Wetering, S. Boyoglu-
1217 Barnum, K. Leung, W. Shi, E.S. Yang, Y. Zhang, J.M. Todd, L. Wang, G.S. Alvarado, H.
1218 Andersen, K.E. Foulds, D.K. Edwards, J.R. Mascola, I.N. Moore, M.G. Lewis, A. Carfi,

1219 D. Montefiori, M.S. Suthar, A. McDermott, M. Roederer, N.J. Sullivan, D.C. Douek,
1220 B.S. Graham, and R.A. Seder. 2021. Immune correlates of protection by mRNA-1273
1221 vaccine against SARS-CoV-2 in nonhuman primates. *Science* 373:eabj0299.
1222 Crawford, K.H.D., R. Eguia, A.S. Dingens, A.N. Loes, K.D. Malone, C.R. Wolf, H.Y. Chu,
1223 M.A. Tortorici, D. Veesler, M. Murphy, D. Pettie, N.P. King, A.B. Balazs, and J.D.
1224 Bloom. 2020. Protocol and Reagents for Pseudotyping Lentiviral Particles with SARS-
1225 CoV-2 Spike Protein for Neutralization Assays. *Viruses* 12:
1226 Crescioli, S., S. Jatiani, and L. Moise. 2025. With great power, comes great responsibility: the
1227 importance of broadly measuring Fc-mediated effector function early in the antibody
1228 development process. *MAbs* 17:2453515.
1229 Cui, L., T. Li, M. Lan, M. Zhou, W. Xue, S. Zhang, H. Wang, M. Hong, Y. Zhang, L. Yuan, H.
1230 Sun, J. Ye, Q. Zheng, Y. Guan, Y. Gu, N. Xia, and S. Li. 2024. A cryptic site in class 5
1231 epitope of SARS-CoV-2 RBD maintains highly conservation across natural isolates.
1232 *iScience* 27:110208.
1233 Fan, C., A.A. Cohen, K.-M.A. Dam, A.V. Rorick, A.-C.I. Priso Fils, Z. Yang, P.N.P.
1234 Gnanapragasam, L.N. Segovia, K.E. Huey-Tubman, W.J. Moon, P.J.C. Lin, P.J.
1235 Bjorkman, and M.A.G. Hoffmann. 2025a. Bivalent mRNA booster encoding virus-like
1236 particles elicits potent polyclass RBD antibodies in pre-vaccinated mice. In eLife
1237 Sciences Publications, Ltd.
1238 Fan, C., A.A. Cohen, M. Park, A.F. Hung, J.R. Keeffe, P.N.P. Gnanapragasam, Y.E. Lee, H.
1239 Gao, L.M. Kakutani, Z. Wu, H. Kleanthous, K.E. Malecek, J.C. Williams, and P.J.
1240 Bjorkman. 2022. Neutralizing monoclonal antibodies elicited by mosaic RBD
1241 nanoparticles bind conserved sarbecovirus epitopes. *Immunity* 55:2419–2435 e2410.
1242 Fan, C., J.R. Keeffe, K.E. Malecek, A.A. Cohen, A.P. West, Jr., V.A. Baharani, A.V. Rorick, H.
1243 Gao, P.N.P. Gnanapragasam, S. Rho, J. Alvarez, L.N. Segovia, T. Hatziioannou, P.D.
1244 Bieniasz, and P.J. Bjorkman. 2025b. Cross-reactive sarbecovirus antibodies induced by
1245 mosaic RBD nanoparticles. *Proc Natl Acad Sci U S A* 122:e2501637122.
1246 Foged, C., B. Brodin, S. Frokjaer, and A. Sundblad. 2005. Particle size and surface charge affect
1247 particle uptake by human dendritic cells in an in vitro model. *Int J Pharm* 298:315–322.
1248 Fumagalli, V., M. Rava, D. Marotta, P. Di Lucia, E.B. Bono, L. Giustini, F. De Leo, M.
1249 Casalgrandi, E. Monteleone, V. Mouro, C. Malpighi, C. Perucchini, M. Grillo, S. De
1250 Palma, L. Donnici, S. Marchese, M. Conti, H. Muramatsu, S. Perlman, N. Pardi, M.
1251 Kuka, R. De Francesco, M.E. Bianchi, L.G. Guidotti, and M. Iannacone. 2024. Antibody-
1252 independent protection against heterologous SARS-CoV-2 challenge conferred by prior
1253 infection or vaccination. *Nat Immunol* 25:633–643.
1254 Gilbert, P.B., D.C. Montefiori, A.B. McDermott, Y. Fong, D. Benkeser, W. Deng, H. Zhou, C.R.
1255 Houchens, K. Martins, L. Jayashankar, F. Castellino, B. Flach, B.C. Lin, S. O'Connell, C.
1256 McDanal, A. Eaton, M. Sarzotti-Kelsoe, Y. Lu, C. Yu, B. Borate, L.W.P. van der Laan,
1257 N.S. Hejazi, C. Huynh, J. Miller, H.M. El Sahly, L.R. Baden, M. Baron, L. De La Cruz,
1258 C. Gay, S. Kalams, C.F. Kelley, M.P. Andrasik, J.G. Kublin, L. Corey, K.M. Neuzil, L.N.
1259 Carpp, R. Pajon, D. Follmann, R.O. Donis, R.A. Koup, s. Immune Assays Team section,
1260 I.T.s.s. Moderna, s. Coronavirus Vaccine Prevention Network /Coronavirus Efficacy
1261 Team section, and V.P.N.B.T.s.s. United States Government /Co. 2022. Immune
1262 correlates analysis of the mRNA-1273 COVID-19 vaccine efficacy clinical trial. *Science*
1263 375:43–50.
1264 Goldblatt, D., G. Alter, S. Crotty, and S.A. Plotkin. 2022. Correlates of protection against SARS-
1265 CoV-2 infection and COVID-19 disease. *Immunol Rev* 310:6–26.
1266 Gonzalez-Magaldi, M., A. Gullapalli, O. Papoulas, C. Liu, A.Y. Leung, L. Guo, A.F. Brilot,
1267 E.M. Marcotte, Z. Ke, and D.J. Leahy. 2025. Structure and organization of full-length

1268 epidermal growth factor receptor in extracellular vesicles by cryo-electron tomography.
1269 *Proc Natl Acad Sci U S A* 122:e2424678122.
1270 Gote, V., P.K. Bolla, N. Kommineni, A. Butreddy, P.K. Nukala, S.S. Palakurthi, and W. Khan.
1271 2023. A Comprehensive Review of mRNA Vaccines. *Int J Mol Sci* 24:
1272 Greaney, A.J., A.N. Loes, K.H.D. Crawford, T.N. Starr, K.D. Malone, H.Y. Chu, and J.D.
1273 Bloom. 2021a. Comprehensive mapping of mutations in the SARS-CoV-2 receptor-
1274 binding domain that affect recognition by polyclonal human plasma antibodies. *Cell Host*
1275 *Microbe* 29:463–476 e466.
1276 Greaney, A.J., A.N. Loes, L.E. Gentles, K.H.D. Crawford, T.N. Starr, K.D. Malone, H.Y. Chu,
1277 and J.D. Bloom. 2021b. Antibodies elicited by mRNA-1273 vaccination bind more
1278 broadly to the receptor binding domain than do those from SARS-CoV-2 infection.
1279 *Science translational medicine* 13:
1280 Greaney, A.J., T.N. Starr, C.O. Barnes, Y. Weisblum, F. Schmidt, M. Caskey, C. Gaebler, A.
1281 Cho, M. Agudelo, S. Finkin, Z. Wang, D. Poston, F. Muecksch, T. Hatziioannou, P.D.
1282 Bieniasz, D.F. Robbiani, M.C. Nussenzweig, P.J. Bjorkman, and J.D. Bloom. 2021c.
1283 Mapping mutations to the SARS-CoV-2 RBD that escape binding by different classes of
1284 antibodies. *Nat Commun* 12:4196.
1285 Greaney, A.J., T.N. Starr, R.T. Eguia, A.N. Loes, K. Khan, F. Karim, S. Cele, J.E. Bowen, J.K.
1286 Logue, D. Corti, D. Veesler, H.Y. Chu, A. Sigal, and J.D. Bloom. 2022. A SARS-CoV-2
1287 variant elicits an antibody response with a shifted immunodominance hierarchy. *PLoS*
1288 *Pathog* 18:e1010248.
1289 Greaney, A.J., T.N. Starr, P. Gilchuk, S.J. Zost, E. Binshtein, A.N. Loes, S.K. Hilton, J.
1290 Huddleston, R. Eguia, K.H.D. Crawford, A.S. Dingens, R.S. Nargi, R.E. Sutton, N.
1291 Suryadevara, P.W. Rothlauf, Z. Liu, S.P.J. Whelan, R.H. Carnahan, J.E. Crowe, Jr., and
1292 J.D. Bloom. 2021d. Complete Mapping of Mutations to the SARS-CoV-2 Spike
1293 Receptor-Binding Domain that Escape Antibody Recognition. *Cell Host Microbe* 29:44–
1294 57 e49.
1295 Guo, L., E. McFadden, M.M. Slough, E.T. Stone, J. Berrigan, E. Mittler, K. Hatzakis, T.
1296 Hinkley, H.S. Kain, Z. Ke, N.L. Warner, J.H. Erasmus, K. Chandran, and J.S. McLellan.
1297 2025. High-resolution in situ structures of hantavirus glycoprotein tetramers. *bioRxiv*
1298 Han, Q., X. Gao, Z. Chu, X. Wang, F. Eisa Addoma Adam, S. Zhang, Y. Jia, X. Qiu, X. Wang,
1299 and Z. Yang. 2019. Truncated chicken MDA5 enhances the immune response to
1300 inactivated NDV vaccine. *Vet Immunol Immunopathol* 208:44–52.
1301 Hendricks, G.G., L. Grigoryan, M.J. Navarro, N.J. Catanzaro, M.L. Hubbard, J.M. Powers, M.
1302 Mattocks, C. Treichel, A.C. Walls, J. Lee, D. Ellis, J.Y.J. Wang, S. Cheng, M.C.
1303 Miranda, A. Valdez, C.W. Chao, S. Chan, C. Men, M.R. Johnson, S.K. Zepeda, S. Ols,
1304 H. Hui, S.Y. Wu, V. Lujan, H. Muramatsu, P.J.C. Lin, M.M.H. Sung, Y.K. Tam, E.M.
1305 Leaf, N. Pardi, R.S. Baric, B. Pulendran, D. Veesler, A. Schafer, and N.P. King. 2025.
1306 Computationally designed mRNA-launched protein nanoparticle immunogens elicit
1307 protective antibody and T cell responses in mice. *Science translational medicine*
1308 17:eadu2085.
1309 Hills, F.R., J.L. Geoghegan, and M. Bostina. 2025. Architects of infection: A structural overview
1310 of SARS-related coronavirus spike glycoproteins. *Virology* 604:110383.
1311 Hills, R.A., T.K. Tan, A.A. Cohen, J.R. Keeffe, A.H. Keeble, P.N.P. Gnanapragasam, K.N.
1312 Storm, A.V. Rorick, A.P. West, Jr., M.L. Hill, S. Liu, J. Gilbert-Jaramillo, M. Afzal, A.
1313 Napier, G. Admans, W.S. James, P.J. Bjorkman, A.R. Townsend, and M.R. Howarth.
1314 2024. Proactive vaccination using multiviral Quartet Nanocages to elicit broad anti-
1315 coronavirus responses. *Nat Nanotechnol* 19:1216–1223.

1316 Hoffmann, M.A.G., Z. Yang, K.E. Huey-Tubman, A.A. Cohen, P.N.P. Gnanapragasam, L.M.
1317 Nakatomi, K.N. Storm, W.J. Moon, P.J.C. Lin, A.P. West, Jr., and P.J. Bjorkman. 2023.
1318 ESCRT recruitment to SARS-CoV-2 spike induces virus-like particles that improve
1319 mRNA vaccines. *Cell* 186:2380–2391 e2389.
1320 Hou, X., T. Zaks, R. Langer, and Y. Dong. 2021. Lipid nanoparticles for mRNA delivery. *Nat*
1321 *Rev Mater* 1–17.
1322 Hsieh, C.L., J.A. Goldsmith, J.M. Schaub, A.M. DiVenere, H.C. Kuo, K. Javanmardi, K.C. Le,
1323 D. Wrapp, A.G. Lee, Y. Liu, C.W. Chou, P.O. Byrne, C.K. Hjorth, N.V. Johnson, J.
1324 Ludes-Meyers, A.W. Nguyen, J. Park, N. Wang, D. Amengor, J.J. Lavinder, G.C.
1325 Ippolito, J.A. Maynard, I.J. Finkelstein, and J.S. McLellan. 2020. Structure-based design
1326 of prefusion-stabilized SARS-CoV-2 spikes. *Science* 369:1501–1505.
1327 Hwang, H.S., Y.T. Lee, K.H. Kim, H.S. Seo, K.S. Yang, H. Cho, and S.M. Kang. 2021. Roles of
1328 the Fc Receptor gamma-Chain in Inducing Protective Immune Responses after
1329 Heterologous Vaccination against Respiratory Syncytial Virus Infection. *Vaccines*
1330 *(Basel)* 9:
1331 Jensen, J.L., R.S. Sankhala, V. Dussupt, H. Bai, A. Hajduczki, K.G. Lal, W.C. Chang, E.J.
1332 Martinez, C.E. Peterson, E.S. Golub, P.A. Rees, L. Mendez-Rivera, M. Zemil, E.
1333 Kavusak, S.V. Mayer, L. Wieczorek, S. Kannan, B.J. Doranz, E. Davidson, E.S. Yang, Y.
1334 Zhang, M. Chen, M. Choe, L. Wang, G.D. Gromowski, R.A. Koup, N.L. Michael, V.R.
1335 Polonis, M. Rolland, K. Modjarrad, S.J. Krebs, and M.G. Joyce. 2023. Targeting the
1336 Spike Receptor Binding Domain Class V Cryptic Epitope by an Antibody with Pan-
1337 Sarbecovirus Activity. *J Virol* 97:e0159622.
1338 Jette, C.A., A.A. Cohen, P.N.P. Gnanapragasam, F. Muecksch, Y.E. Lee, K.E. Huey-Tubman, F.
1339 Schmidt, T. Hatziioannou, P.D. Bieniasz, M.C. Nussenzweig, A.P. West, J.R. Keeffe, P.J.
1340 Bjorkman, and C.O. Barnes. 2021. Broad cross-reactivity across sarbecoviruses exhibited
1341 by a subset of COVID-19 donor-derived neutralizing antibodies. *Cell reports* 36:109760.
1342 Joshi, V.B., S.M. Geary, and A.K. Salem. 2013. Biodegradable particles as vaccine delivery
1343 systems: size matters. *AAPS J* 15:85–94.
1344 Kim, C., J.D. Kim, and S.U. Seo. 2022. Nanoparticle and virus-like particle vaccine approaches
1345 against SARS-CoV-2. *J Microbiol* 60:335–346.
1346 Kleanthous, H., J.M. Silverman, K.W. Makar, I.K. Yoon, N. Jackson, and D.W. Vaughn. 2021.
1347 Scientific rationale for developing potent RBD-based vaccines targeting COVID-19. *NPJ*
1348 *Vaccines* 6:128.
1349 Landau, M., I. Mayrose, Y. Rosenberg, F. Glaser, E. Martz, T. Pupko, and N. Ben-Tal. 2005.
1350 ConSurf 2005: the projection of evolutionary conservation scores of residues on protein
1351 structures. *Nucleic Acids Res* 33:W299–302.
1352 Leehan, K.M., and K.A. Koelsch. 2015. T Cell ELISPOT: For the Identification of Specific
1353 Cytokine-Secreting T Cells. *Methods Mol Biol* 1312:427–434.
1354 Lehle, L., and E. Bause. 1984. Primary structural requirements for N- and O-glycosylation of
1355 yeast mannoproteins. *Biochimica et Biophysica Acta (BBA) - General Subjects* 799:246–
1356 251.
1357 McBride, C.E., J. Li, and C.E. Machamer. 2007. The cytoplasmic tail of the severe acute
1358 respiratory syndrome coronavirus spike protein contains a novel endoplasmic reticulum
1359 retrieval signal that binds COPI and promotes interaction with membrane protein. *J Virol*
1360 81:2418–2428.
1361 McInnes, L., J. Healy, and J. Melville. 2020. UMAP: Uniform Manifold Approximation and
1362 Projection for Dimension Reduction, v3. In.
1363 Morris, G.E. 1996. Epitope Mapping of Protein Antigens by Competition ELISA. In The Protein
1364 Protocols Handbook. 595–600.

1365 Olson, B.A., K.E. Huey-Tubman, Z. Mao, M.A.G. Hoffmann, P.J. Bjorkman, R.M. Murray, and
1366 S.L. Mayo. 2025. Recruiting ESCRT to single-chain heterotrimer peptide MHCI releases
1367 antigen-presenting vesicles that stimulate T cells selectively. *Proc Natl Acad Sci U S A*
1368 122:e2501046122.
1369 Paciello, I., G. Maccari, E. Pantano, E. Andreano, and R. Rappuoli. 2024. High-resolution map
1370 of the Fc functions mediated by COVID-19-neutralizing antibodies. *Proc Natl Acad Sci*
1371 *U S A* 121:e2314730121.
1372 Pardi, N., M.J. Hogan, F.W. Porter, and D. Weissman. 2018. mRNA vaccines - a new era in
1373 vaccinology. *Nat Rev Drug Discov* 17:261–279.
1374 Pardi, N., S. Tuyishime, H. Muramatsu, K. Kariko, B.L. Mui, Y.K. Tam, T.D. Madden, M.J.
1375 Hope, and D. Weissman. 2015. Expression kinetics of nucleoside-modified mRNA
1376 delivered in lipid nanoparticles to mice by various routes. *J Control Release* 217:345–
1377 351.
1378 Rahikainen, R., P. Rijal, T.K. Tan, H.J. Wu, A.C. Andersson, J.R. Barrett, T.A. Bowden, S.J.
1379 Draper, A.R. Townsend, and M. Howarth. 2021. Overcoming Symmetry Mismatch in
1380 Vaccine Nanoassembly through Spontaneous Amidation. *Angew Chem Int Ed Engl*
1381 60:321–330.
1382 Ranieri, E., I. Popescu, and M. Gigante. 2014. CTL ELISPOT assay. *Methods Mol Biol*
1383 1186:75–86.
1384 Robbiani, D.F., C. Gaebler, F. Muecksch, J.C.C. Lorenzi, Z. Wang, A. Cho, M. Agudelo, C.O.
1385 Barnes, A. Gazumyan, S. Finkin, T. Hagglof, T.Y. Oliveira, C. Viant, A. Hurley, H.H.
1386 Hoffmann, K.G. Millard, R.G. Kost, M. Cipolla, K. Gordon, F. Bianchini, S.T. Chen, V.
1387 Ramos, R. Patel, J. Dizon, I. Shimeliovich, P. Mendoza, H. Hartweger, L. Nogueira, M.
1388 Pack, J. Horowitz, F. Schmidt, Y. Weisblum, E. Michailidis, A.W. Ashbrook, E. Waltari,
1389 J.E. Pak, K.E. Huey-Tubman, N. Koranda, P.R. Hoffman, A.P. West, Jr., C.M. Rice, T.
1390 Hatziioannou, P.J. Bjorkman, P.D. Bieniasz, M. Caskey, and M.C. Nussenzweig. 2020.
1391 Convergent antibody responses to SARS-CoV-2 in convalescent individuals. *Nature*
1392 584:437–442.
1393 Rock, K.L., E. Reits, and J. Neefjes. 2016. Present Yourself! By MHC Class I and MHC Class II
1394 Molecules. *Trends Immunol* 37:724–737.
1395 Roederer, A.L., Y. Cao, K. St Denis, M.L. Sheehan, C.J. Li, E.C. Lam, D.J. Gregory, M.C.
1396 Poznansky, A.J. Iafrate, D.H. Canaday, S. Gravenstein, W.F. Garcia-Beltran, and A.B.
1397 Balazs. 2024. Ongoing evolution of SARS-CoV-2 drives escape from mRNA vaccine-
1398 induced humoral immunity. *Cell Rep Med* 5:101850.
1399 Schmidt, F., Y. Weisblum, F. Muecksch, H.-H. Hoffmann, E. Michailidis, J.C.C. Lorenzi, P.
1400 Mendoza, M. Rutkowska, E. Bednarski, C. Gaebler, M. Agudelo, A. Cho, Z. Wang, A.
1401 Gazumyan, M. Cipolla, M. Caskey, D.F. Robbiani, M.C. Nussenzweig, C.M. Rice, T.
1402 Hatziioannou, and P.D. Bieniasz. 2020. Measuring SARS-CoV-2 neutralizing antibody
1403 activity using pseudotyped and chimeric viruses. *Journal of Experimental Medicine* 217:
1404 Seifert, S.N., S. Bai, S. Fawcett, E.B. Norton, K.J. Zwezdaryk, J. Robinson, B. Gunn, and M.
1405 Letko. 2022. An ACE2-dependent Sarbecovirus in Russian bats is resistant to SARS-
1406 CoV-2 vaccines. *PLoS Pathog* 18:e1010828.
1407 Sievers, F., A. Wilm, D. Dineen, T.J. Gibson, K. Karplus, W. Li, R. Lopez, H. McWilliam, M.
1408 Remmert, J. Soding, J.D. Thompson, and D.G. Higgins. 2011. Fast, scalable generation
1409 of high-quality protein multiple sequence alignments using Clustal Omega. *Mol Syst Biol*
1410 7:539.
1411 Starr, T.N., N. Czudnochowski, Z. Liu, F. Zatta, Y.J. Park, A. Addetia, D. Pinto, M. Beltramello,
1412 P. Hernandez, A.J. Greaney, R. Marzi, W.G. Glass, I. Zhang, A.S. Dingens, J.E. Bowen,
1413 M.A. Tortorici, A.C. Walls, J.A. Wojcechowskyj, A. De Marco, L.E. Rosen, J. Zhou, M.

1414 Montiel-Ruiz, H. Kaiser, J.R. Dillen, H. Tucker, J. Bassi, C. Silacci-Fregni, M.P.
1415 Housley, J. di Iulio, G. Lombardo, M. Agostini, N. Sprugasci, K. Culap, S. Jaconi, M.
1416 Meury, E. Dellota, Jr., R. Abdelnabi, S.C. Foo, E. Cameroni, S. Stumpf, T.I. Croll, J.C.
1417 Nix, C. Havenar-Daughton, L. Piccoli, F. Benigni, J. Neyts, A. Telenti, F.A. Lempp,
1418 M.S. Pizzuto, J.D. Chodera, C.M. Hebner, H.W. Virgin, S.P.J. Whelan, D. Veesler, D.
1419 Corti, J.D. Bloom, and G. Snell. 2021a. SARS-CoV-2 RBD antibodies that maximize
1420 breadth and resistance to escape. *Nature* 597:97–102.
1421 Starr, T.N., A.J. Greaney, A. Addetia, W.W. Hannon, M.C. Choudhary, A.S. Dingens, J.Z. Li,
1422 and J.D. Bloom. 2021b. Prospective mapping of viral mutations that escape antibodies
1423 used to treat COVID-19. *Science* 371:850–854.
1424 Starr, T.N., A.J. Greaney, W.W. Hannon, A.N. Loes, K. Hauser, J.R. Dillen, E. Ferri, A.G.
1425 Farrell, B. Dadonaite, M. McCallum, K.A. Matreyek, D. Corti, D. Veesler, G. Snell, and
1426 J.D. Bloom. 2022. Shifting mutational constraints in the SARS-CoV-2 receptor-binding
1427 domain during viral evolution. *Science* 377:420–424.
1428 Starr, T.N., A.J. Greaney, S.K. Hilton, D. Ellis, K.H.D. Crawford, A.S. Dingens, M.J. Navarro,
1429 J.E. Bowen, M.A. Tortorici, A.C. Walls, N.P. King, D. Veesler, and J.D. Bloom. 2020.
1430 Deep Mutational Scanning of SARS-CoV-2 Receptor Binding Domain Reveals
1431 Constraints on Folding and ACE2 Binding. *Cell* 182:1295–1310.e1220.
1432 Stewart-Jones, G.B.E., S.M. Elbashir, K. Wu, D. Lee, I. Renzi, B. Ying, M. Koch, C.E. Sein, A.
1433 Choi, B. Whitener, D. Garcia-Dominguez, C. Henry, A. Woods, L. Ma, D. Montes
1434 Berrueta, L.E. Avena, J. Quinones, S. Falcone, C.J. Hsiao, S.M. Scheaffer, L.B.
1435 Thackray, P. White, M.S. Diamond, D.K. Edwards, and A. Carfi. 2023. Domain-based
1436 mRNA vaccines encoding spike protein N-terminal and receptor binding domains confer
1437 protection against SARS-CoV-2. *Science translational medicine* 15:eadf4100.
1438 Turner, H.L., A.M. Jackson, S.T. Richey, L.M. Sewall, A. Antanasijevic, L. Hangartner, and
1439 A.B. Ward. 2023. Protocol for analyzing antibody responses to glycoprotein antigens
1440 using electron-microscopy-based polyclonal epitope mapping. *STAR Protoc* 4:102476.
1441 Tykvart, J., P. Sacha, C. Barinka, T. Knedlik, J. Starkova, J. Lubkowski, and J. Konvalinka.
1442 2012. Efficient and versatile one-step affinity purification of in vivo biotinylated proteins:
1443 expression, characterization and structure analysis of recombinant human glutamate
1444 carboxypeptidase II. *Protein Expr Purif* 82:106–115.
1445 Votteler, J., and W.I. Sundquist. 2013. Virus budding and the ESCRT pathway. *Cell Host*
1446 *Microbe* 14:232–241.
1447 Walker, S.E., and J. Lorsch. 2013. RNA purification--precipitation methods. *Methods Enzymol*
1448 530:337–343.
1449 Wang, E., A.A. Cohen, L.F. Caldera, J.R. Keeffe, A.V. Rorick, Y.M. Adia, P.N.P.
1450 Gnanapragasam, P.J. Bjorkman, and A.K. Chakraborty. 2025. Designed mosaic
1451 nanoparticles enhance cross-reactive immune responses in mice. *Cell* 188:1036–1050
1452 e1011.
1453 Wang, Z., F. Muecksch, A. Cho, C. Gaebler, H.H. Hoffmann, V. Ramos, S. Zong, M. Cipolla, B.
1454 Johnson, F. Schmidt, J. DaSilva, E. Bednarski, T. Ben Tanfous, R. Raspe, K. Yao, Y.E.
1455 Lee, T. Chen, M. Turroja, K.G. Milard, J. Dizon, A. Kaczynska, A. Gazumyan, T.Y.
1456 Oliveira, C.M. Rice, M. Caskey, P.D. Bieniasz, T. Hatziioannou, C.O. Barnes, and M.C.
1457 Nussenzweig. 2022. Analysis of memory B cells identifies conserved neutralizing
1458 epitopes on the N-terminal domain of variant SARS-Cov-2 spike proteins. *Immunity*
1459 55:998–1012 e1018.
1460 West, A.P., Jr., L. Scharf, J. Horwitz, F. Klein, M.C. Nussenzweig, and P.J. Bjorkman. 2013.
1461 Computational analysis of anti-HIV-1 antibody neutralization panel data to identify
1462 potential functional epitope residues. *Proc Natl Acad Sci U S A* 110:10598–10603.

1463 Whittaker, C., G. Barnsley, D.O. Mesa, V. Cox, D.J. Laydon, C.W. Tan, F. Zhu, R. Johnson, P.
1464 Doohan, L.K. Whittles, G. Nedjati-Gilani, P. Winskill, A.B. Hogan, A. Deol, C.
1465 Mukandavire, K. Hauck, D.C.B. Lye, L.F. Wang, O.J. Watson, and A.C. Ghani. 2025.
1466 Quantifying the impact of a broadly protective sarbecovirus vaccine in a future SARS-X
1467 pandemic. *Nat Commun* 16:8495.
1468 Wong, B.K., and N.A. Mabbott. 2024. Systematic review and meta-analysis of COVID-19
1469 mRNA vaccine effectiveness against hospitalizations in adults. *Immunother Adv*
1470 4:ltae011.
1471 Zepeda-Cervantes, J., J.O. Ramirez-Jarquin, and L. Vaca. 2020. Interaction Between Virus-Like
1472 Particles (VLPs) and Pattern Recognition Receptors (PRRs) From Dendritic Cells (DCs):
1473 Toward Better Engineering of VLPs. *Front Immunol* 11:1100.
1474 Zhang, Y., C. Wang, Y. Zheng, F. Chen, Y. Feng, L. Fang, Z. Wang, Z.F. Fu, M. Zhou, and L.
1475 Zhao. 2025. A chimeric Ad5-Envp-VLP vaccine platform confers broad-spectrum 1
1476 immunity against emerging and re-emerging pathogens *bioRxiv*
1477
1478

1479 Supplementary Information for

1480
1481
1482

Genetic encoding of mosaic-8 pan-sarbecovirus RBD vaccine for mRNA delivery

1483 Alexander A. Cohen[1], Jennifer R. Keeffe[1], Lusineh Manasyan[1], Indeever Madireddy[1],
1484 Ange-Célia I. Priso Fils[1], Kim-Marie A. Dam[2], Haley E. Stober[2], Rory A. Hills[,3,4,7], Woohyun J.
1485 Moon[5], Paulo J.C. Lin[5], Mark R. Howarth[3], Magnus A.G. Hoffmann[2,6,8*], Pamela J. Bjorkman[1,8*]

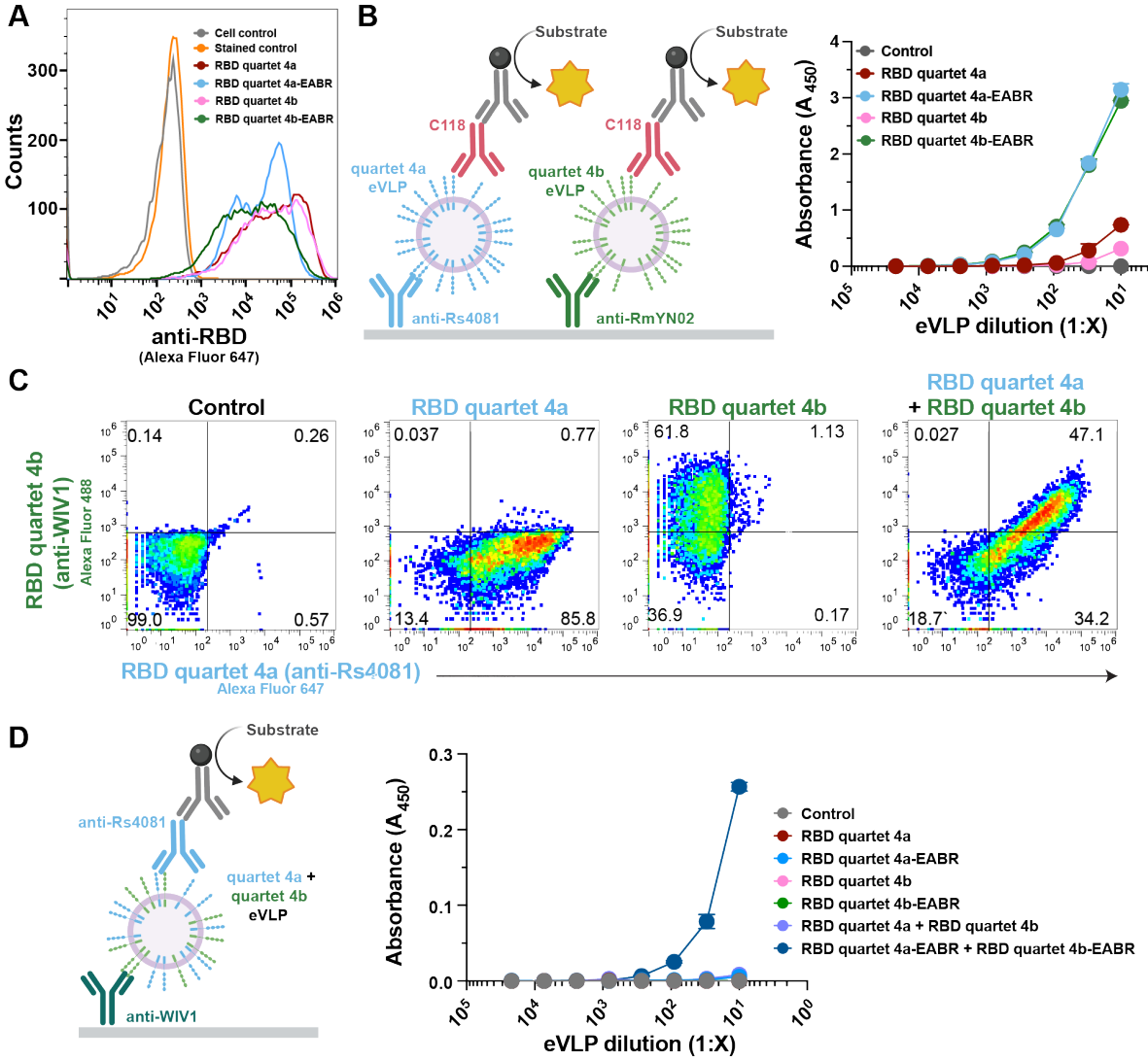

Figure S1. mRNA-encoded dual quartets are presented on cells and eVLPs.
(A) Flow cytometry using C118, a human pan-sarbecovirus RBD-specific mAb (Jette et al., 2021; Robbiani et al., 2020), demonstrating that transfections of mRNAs encoding EABR and non-EABR versions of RBD quartet 4a or quartet 4b resulted in expression on the surface of transfected cells. Untransfected cells are shown as controls (unstained or stained with C118). (B) Left: ELISA schematic. RBD quartet levels were measured by capturing purified eVLPs with an anti-Rs4081 RBD mAb (Fan et al., 2025b) (recognizes RBD quartet 4a but not quartet 4b) or an anti-RmYN02 RBD mAb (Fan et al., 2025b) (recognizes RBD quartet 4b but not quartet 4a) and detecting with the pan-sarbecovirus RBD-specific C118 mAb (Jette et al., 2021; Robbiani et al., 2020). Right: ELISA showing that purified single quartet eVLPs purified from supernatants of cells transfected with mRNA encoding RBD quartet 4a-EABR or RBD quartet 4b-EABR displayed RBD quartets on their surface. The mean absorbance of two replicates is shown as a function of eVLP dilution with error bars representing standard deviations. (C) Flow cytometry demonstrating that RBD quartets 4a and 4b were co-expressed on the surfaces of individual cells. RBD quartet 4a was detected using an anti-Rs4081 RBD mAb (Fan et al., 2025b) and RBD quartet 4b was detected using anti-WIV1 RBD mAb (Fan et al., 2022). Untransfected cells stained with the anti-Rs4081 and anti-WIV1 RBD mAbs are shown as controls. The percentage of cells in each quadrant is shown. (D) Left: ELISA schematic. Purified eVLPs were evaluated in a sandwich ELISA in which

1506 an anti-WIV1 RBD mAb (Fan et al., 2022) (recognizes RBD quartet 4b but not quartet 4a) was
1507 used as a capture Ab and an anti-Rs4081 RBD mAb (Fan et al., 2025b) (recognizes quartet 4a but
1508 not quartet 4b) was used for detection. Right: ELISA showing detection of both RBD quartets 4a
1509 and 4b on the surfaces of eVLPs purified from supernatants of cells co-transfected with mRNAs
1510 encoding RBD quartet 4a-EABR and 4b-EABR constructs. The mean absorbance of two replicates
1511 is shown as a function of eVLP dilution with error bars representing standard deviations. Binding
1512 was not detected for purified supernatant samples from untransfected cells (control) or from
1513 supernatants from cells transfected with RBD quartet 4a, RBD quartet 4a-EABR, RBD quartet 4b,
1514 RBD quartet 4b-EABR, or RBD quartet 4a plus RBD quartet 4b (all data were plotted but some
1515 data points near 0.0 A_{450} are obscured by others).
1516

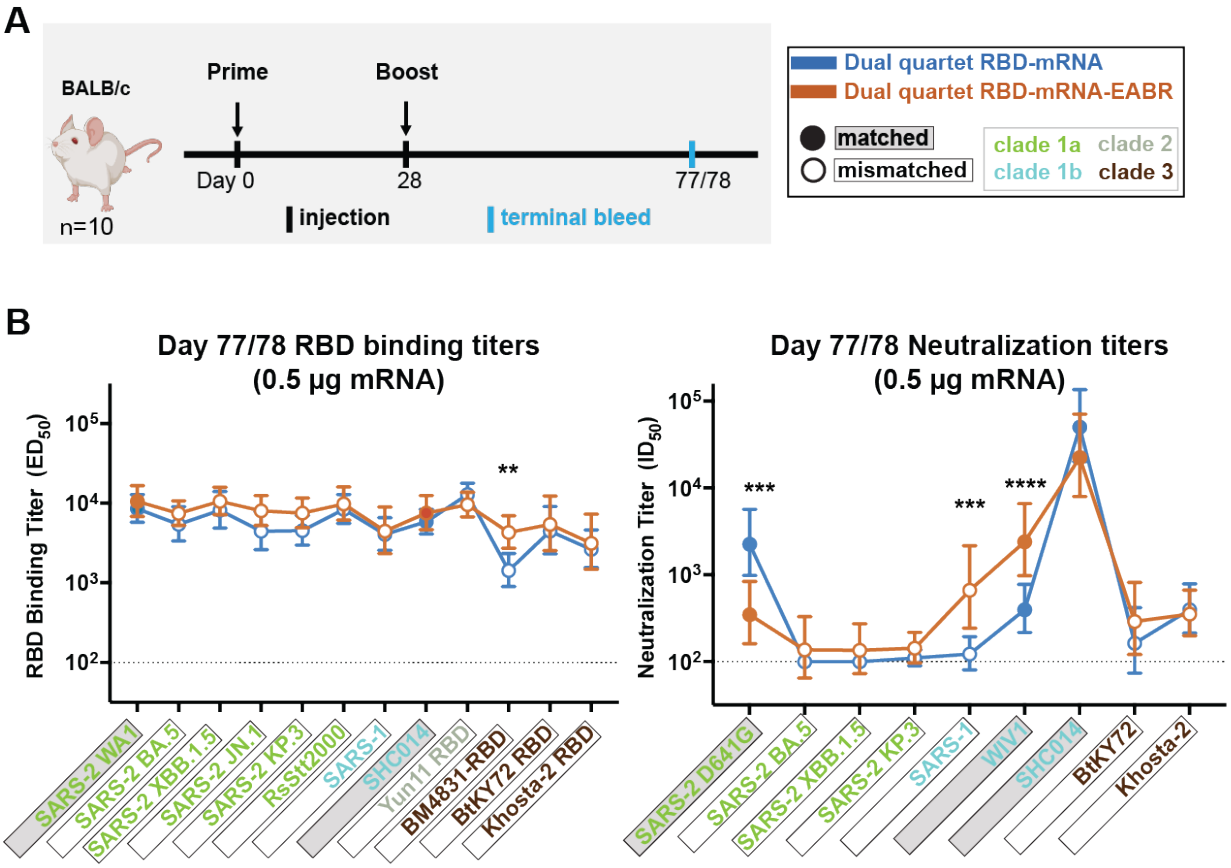

Figure S2. Dual quartet mRNAs elicited cross-reactive Abs.
Data are shown for ELISA and neutralization analyses for terminal bleed serum samples (see also Fig. 2). (A) Immunization regimen. Left: Mice were primed at day 0, boosted at day 28, and samples were collected from a terminal bleed at day 77 or 78. Right: Colors used to identify immunizations and symbols indicating a matched (filled in square data points; gray shading around name) or mismatched (unfilled square data points; black outline around name) sarbecovirus antigen. Sarbecovirus strain names are colored in panel B according to clade. (B) RBD-binding ELISA (left) and pseudovirus neutralization (right) results for serum samples from day 77 or 78 after the prime immunization. Immunogens are shown compared with the cohorts immunized with 0.5 µg of an mRNA-based immunogen. Dashed horizontal lines indicate the limits of detection for each assay. Left: Geomeans of ED_{50} values for animals in each cohort (symbols with geometric standard deviations indicated by error bars) are connected by colored lines. Mean titers against RBDs from indicated sarbecoviruses were compared pairwise across immunization cohorts by Tukey's multiple comparison test with the Geisser-Greenhouse correction (as calculated by GraphPad Prism). Right: Neutralization potencies for serum samples from day 77 or 78 after immunization presented as half-maximal inhibitory dilutions (ID_{50} values) of sera against pseudoviruses from the indicated coronavirus strains. Significant differences between the two cohorts are indicated by asterisks: $p<0.05$ = *, $p<0.01$ = **, $p<0.001$ = ***, $p<0.0001$ = ****.

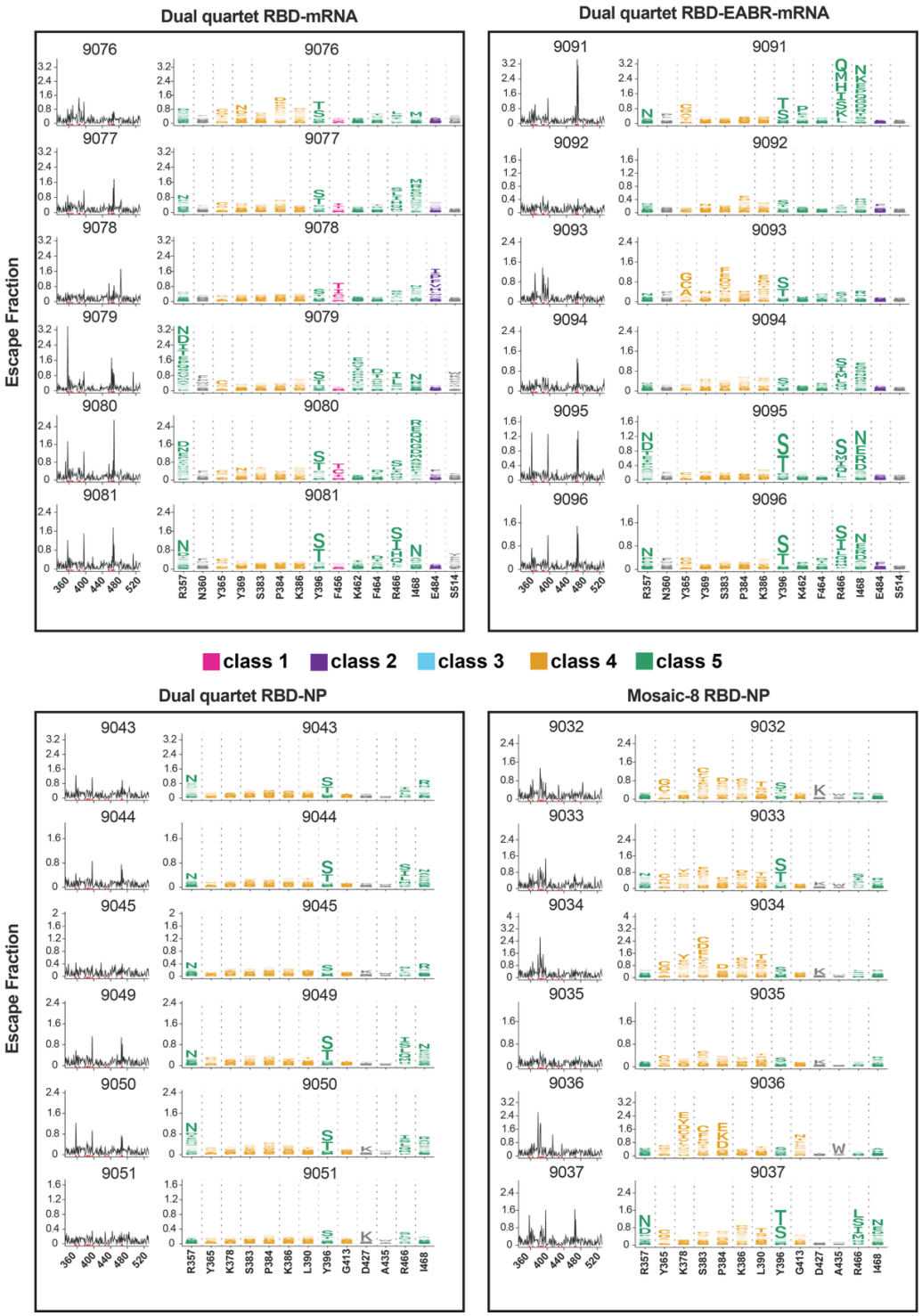

Figure S3. DMS line and logo plots (WA1 RBD library) for individual mice.
DMS line plots (left) and logo plots (right) for results from individual mice (identified by 4-digit numbers) immunized with the indicated immunogens. X-axes of line and logo plots show RBD residue numbers, and y-axes of line plots show the sum of the Ab escape for all substitutions at an RBD residue (larger numbers indicate increased Ab escape). Sites with the strongest Ab escape are shown in logo plots; tall letters represent the most frequent substitutions at a site. Logo plot residues are colored according to RBD epitopes within different classes (Barnes et al., 2020; Cui et al., 2024; Jensen et al., 2023; Jette et al., 2021) as indicated on the legend.

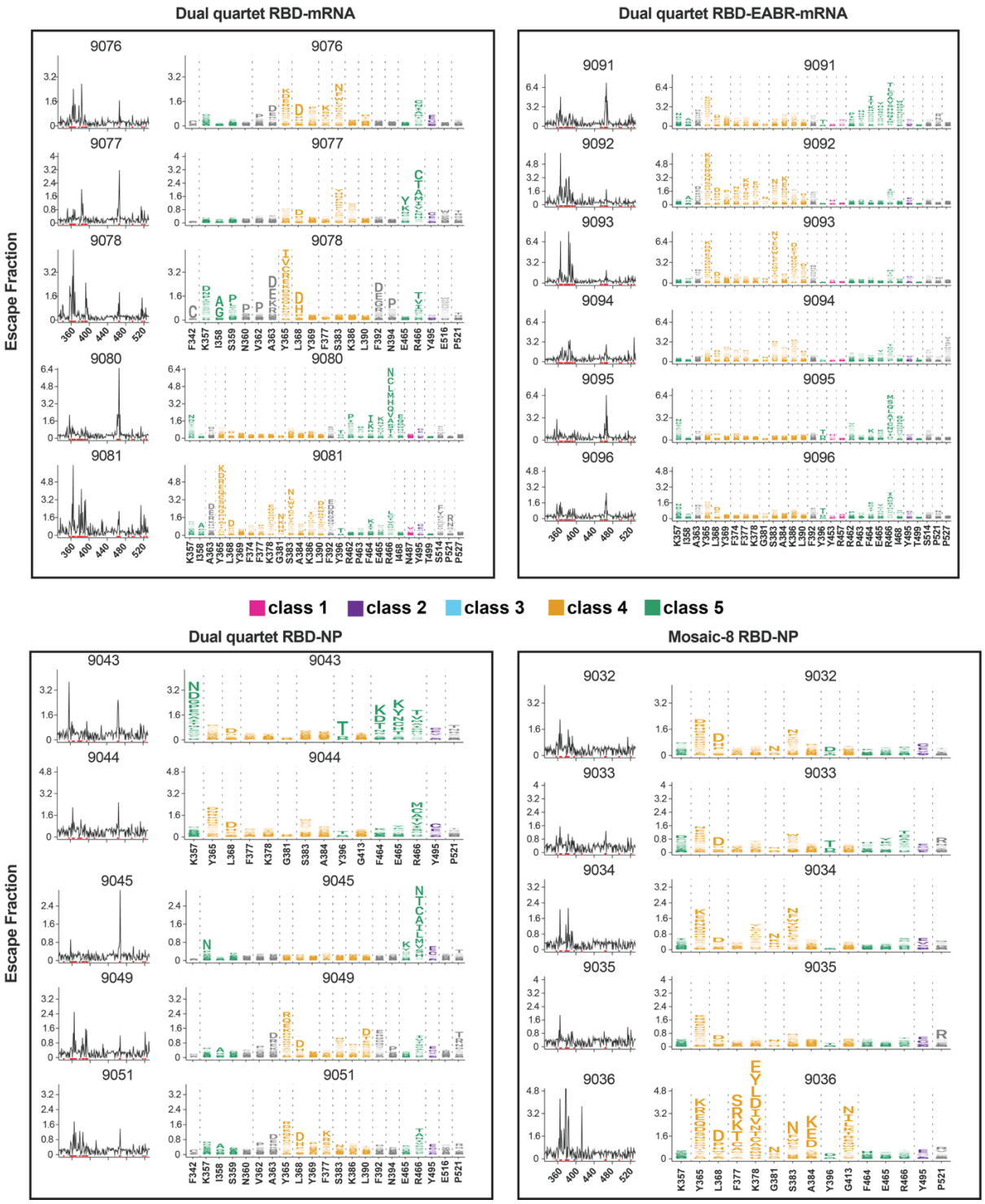

Figure S4. DMS line and logo plots (SARS-1 RBD library) for individual mice.
DMS line plots (left) and logo plots (right) for results from individual mice (identified by 4-digit numbers) immunized with the indicated immunogens. X-axes of line and logo plots show RBD residue numbers, and y-axes of line plots show the sum of the Ab escape for all substitutions at an RBD residue (larger numbers indicate increased Ab escape). Sites with the strongest Ab escape are shown in logo plots; tall letters represent the most frequent substitutions at a site. Logo plot residues are colored according to RBD epitopes within different classes (Barnes et al., 2020; Cui et al., 2024; Jensen et al., 2023; Jette et al., 2021) as indicated on the legend.

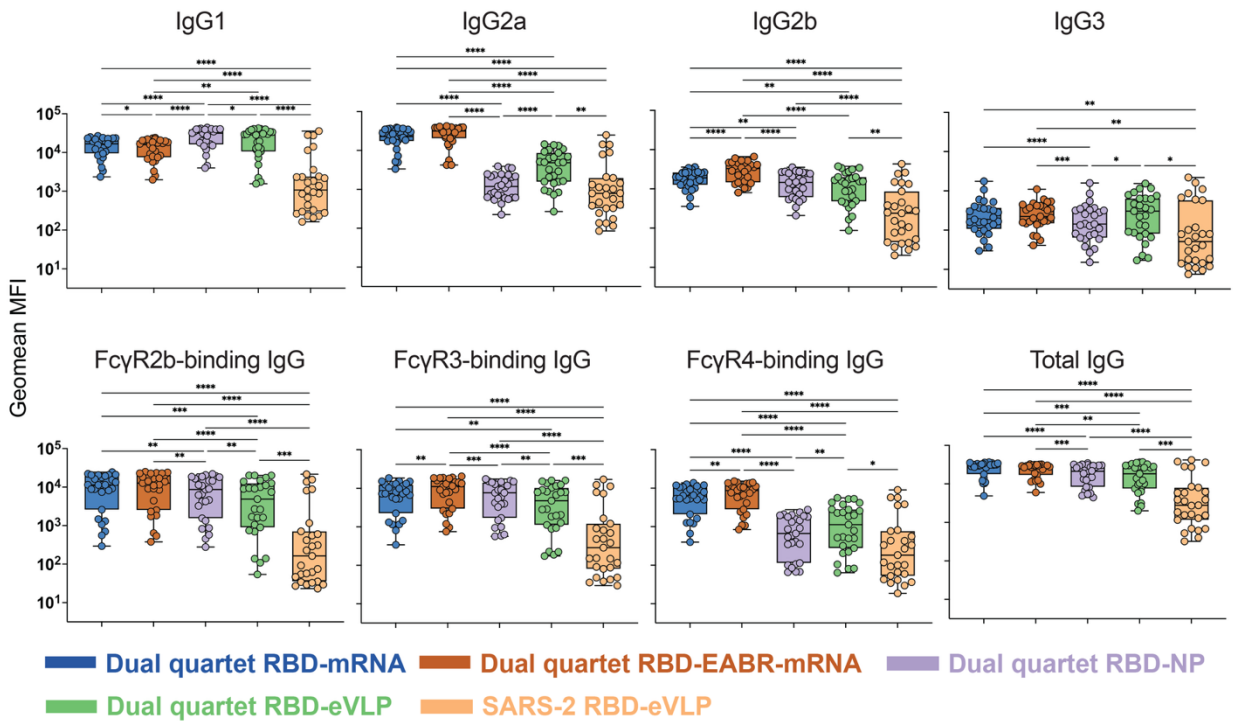

Figure S5. mRNA-encoded dual quartet RBD immunogens elicit balanced IgG subclass and potent FcγR-binding responses.

MFI = Median fluorescent intensity. For IgG1, IgG2a, IgG2b, IgG3, FcγR2b-binding IgGs, FcγR3-binding IgGs, FcγR4-binding IgGs, and total IgG, geomean MFI values of the individual responses shown in panel A for each cohort binding to different spikes or RBDs are represented as points in a box and whisker plot and compared pairwise across immunization cohorts by Tukey's multiple comparison test calculated by GraphPad Prism. Significant differences between cohorts linked by vertical lines in panels B and C are indicated by asterisks: $p<0.05$ = *, $p<0.01$ = **, $p<0.001$ = ***, $p<0.0001$ = ****.

See also Fig. 5.

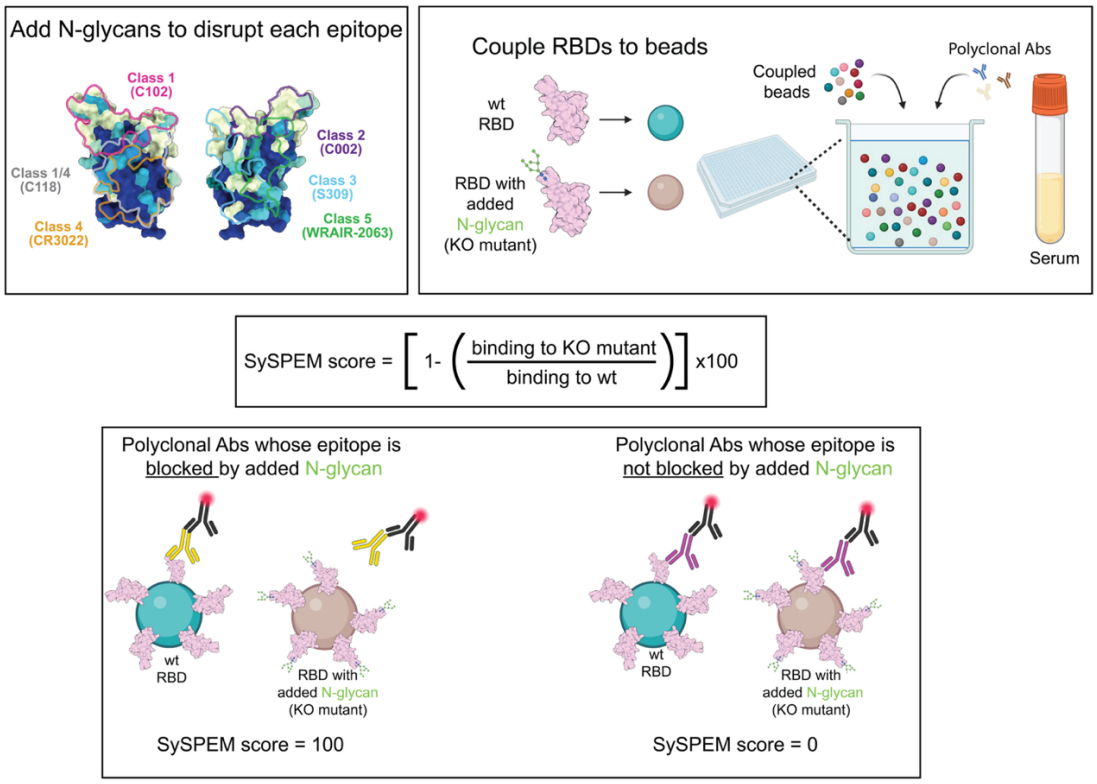

1571

1572 **Figure S6. Schematic of SySPEM approach.**

1573

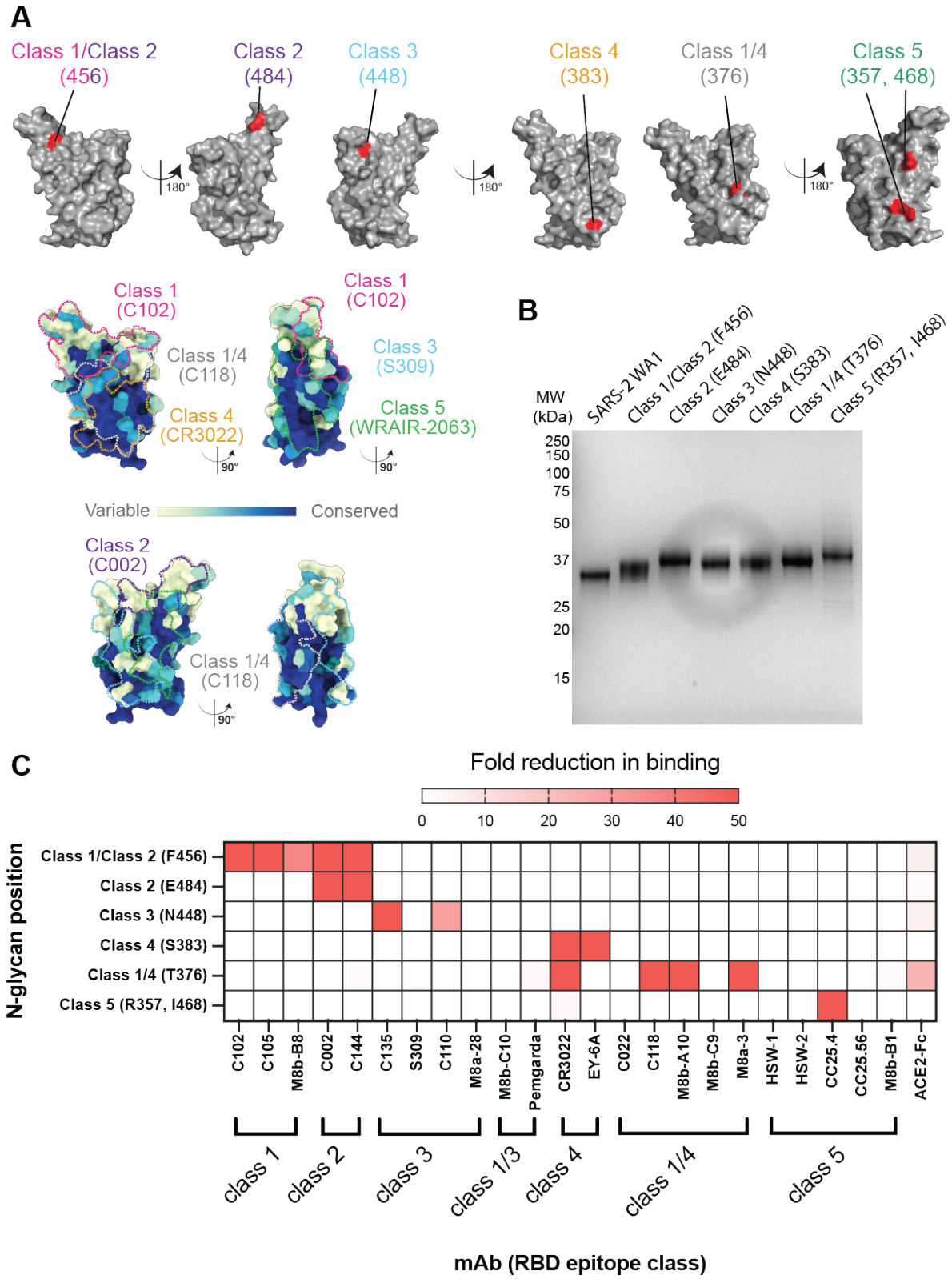

1574
1575 **Figure S7. Characterization of RBD N-glycan mutants used for SySPEM analysis.**
1576 (A) Top: Locations of the added N-glycan(s) in RBD KO mutants, as shown by highlighting of
1577 one or more residues that were changed to Asn in the introduced PNGS(s). Bottom: Sequence
1578 conservation of 16 sarbecovirus RBDs calculated using ConSurf (Landau et al., 2005) shown on a

1579 surface representation of SARS-2 RBD (PDB 7BZ5). Class 1, 2, 3, 4, 1/4, and 5 anti-RBD Ab
1580 epitopes (Barnes et al., 2020; Cui et al., 2024; Jensen et al., 2023; Jette et al., 2021) are outlined in
1581 dots in different colors using information from representative structures of Abs bound to SARS-2
1582 spike or RBD (C102: PDB 7K8M; C002: PDB 7K8T, S309: PDB 7JX3; CR3022: PDB 7LOP;
1583 C118: PDB 7RKV; WRAIR-2063: PDB 8EOO). (B) SDS-PAGE analysis of purified wt RBD and
1584 RBD KO mutants. Molecular weight marker positions are shown on the left with the molecular
1585 weight indicated in kilodaltons. KO mutants are listed with the RBD epitope class affected by the
1586 N-glycan addition(s) and residue number(s) of Asn residue(s) to which N-linked glycan(s) were
1587 added. (C) Results of ELISA showing ratio of binding of characterized mAbs or human ACE2-Fc
1588 (Jette et al., 2021) to wt RBD versus the RBD KO mutants listed on the left. ELISA EC_{50} values
1589 for binding of each reagent to wt RBD and the six RBD KO mutants were derived using , and the
1590 fold reduction in binding to each RBD KO mutant was calculated as EC_{50} RBD KO / EC_{50} RBD
1591 wt. Classifications of RBD epitopes recognized by the characterized mAbs and ACE-2 Fc are
1592 taken from (Barnes et al., 2020; Cui et al., 2024; Fan et al., 2022; Fan et al., 2025b; Jensen et al.,
1593 2023; Jette et al., 2021).

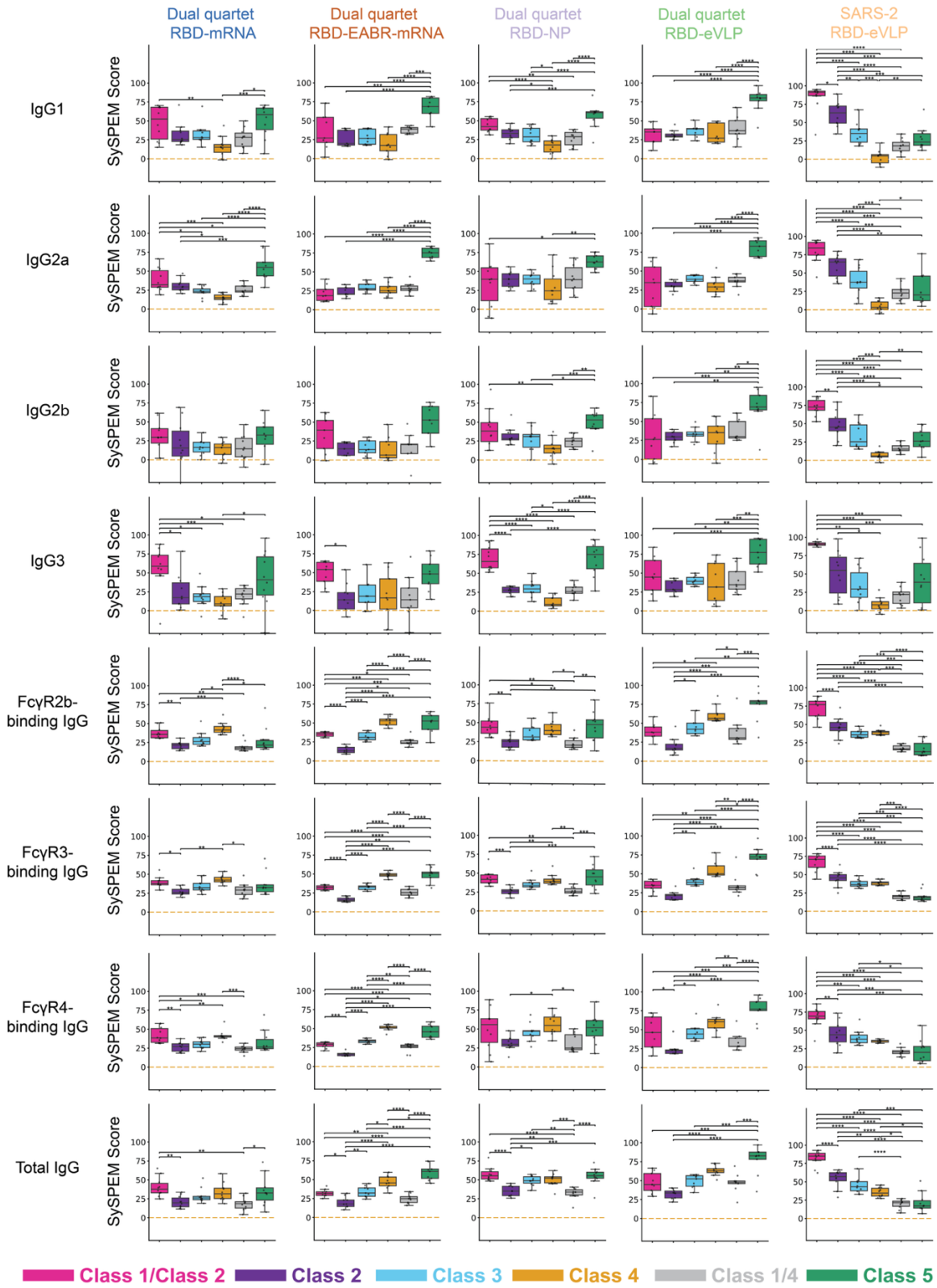

Figure S8. SySPEM score comparisons show distinct epitope profiles across immunogen cohorts.

SySPEM scores from individual mice in each immunogen cohort (columns) were determined for each IgG class (rows, IgG subclass plus different FcγR-binding IgGs) with statistical comparisons

between targeted epitopes (colors). A SySPEM value of 0 indicates that none of the IgGs in that sample were affected by the glycan addition and therefore the sample did not contain IgGs that recognize that epitope, and a SySPEM value of 100 indicates that all IgGs in that sample recognized that epitope (Fig. S6). A SySPEM value between 0 and 100 indicates the proportion of IgGs in a sample that recognized the epitope that was blocked by glycan addition in the RBD KO mutant. Box and whisker plots of SySPEM scores with individual data points representing one mouse are shown. Significant differences between cohorts were calculated using Tukey's HSD posthoc test and linked by vertical lines indicated by asterisks: $p<0.05$ = *, $p<0.01$ = **, $p<0.001$ = ***, $p<0.0001$ = ****. See also Figs. 6 and 7.